Stationary Inverted Balmer and Lyman Populations for a CW HI Water-Plasma Laser

R. Mills*[1], P. Ray[1], R. M. Mayo[1]

Abstract

Stationary inverted H Balmer and Lyman populations were observed from a low pressure water-vapor microwave discharge plasma. The ionization and population of excited atomic hydrogen levels was attributed to energy provided by a catalytic resonance energy transfer between hydrogen atoms and molecular oxygen formed in the water plasma. The catalysis mechanism was supported by the observation of O^{2+} and H Balmer line broadening of 55 eV compared to 1 eV for hydrogen alone. The high hydrogen atom temperature with a relatively low electron temperature, $T_e = 2\,eV$, exhibited characteristics of cold recombining plasmas. These conditions of a water plasma favored an inverted population in the lower levels. Thus, the catalysis of atomic hydrogen may pump a cw HI laser. From our results, laser oscillations are may be possible from i) $n=3$, $n=4$, $n=5$, $n=6$, $n=7$ and $n=8$ to $n=2$, ii) $n=4$, $n=5$, $n=6$, and $n=7$ to $n=3$ and iii) $n=5$ and $n=6$ to $n=4$. Lines of the Balmer series of $n=5$, and $n=6$ to $n=2$ and the Paschen series of $n=5$ to $n=3$ were of particular importance because of the potential to design blue and 1.3 micron infrared lasers, respectively, which are ideal for many communications and microelectronics applications. At a microwave input power of $9\,W \cdot cm^{-3}$, a collisional radiative model showed that the hydrogen excited state population distribution was consistent with an $n=1 \rightarrow 5,6$ pumping power of an unprecedented $200\,W \cdot cm^{-3}$. High power hydrogen gas lasers are anticipated at wavelengths, over a broad spectral range from far infrared to violet which may be miniaturized to micron dimensions. Such a hydrogen laser represents the first new atomic gas laser in over a decade, and it may prove to be the most efficient, versatile, and useful of all. A further application is the direct generation of electrical power using photovoltaic conversion of the spontaneous or stimulated water vapor plasma emission.

[1] BlackLight Power, Inc., 493 Old Trenton Road, Cranbury, NJ 08512

* To whom correspondence should be addressed. Phone: 609-490-1090; Fax: 609-490-1066; E-mail: rmills@blacklightpower.com

1. Introduction

For the last fifteen years there has been an aggressive search for a blue laser. A blue laser would significantly improve the performance of many applications and open new venues. Blue lasers that are durable and bright have significant applications such as superior displays, optical sensors, laser printers and scanners, fiber optical and undersea optical communications, satellite and undersea detection and targeting of submarines, undersea mine detection, undersea salvage, medical devices, and higher density compact disk (CD) players. The shorter (blue) wavelength could be more sharply focused such that the capacity of magnetic and optical storage may be increased. Digital versatile disks (DVDs) which rely on red aluminum indium gallium phosphide (AlInGaP) semiconductor lasers have a data capacity of about 4.7 gigabytes (Gbytes) compared to 0.65 for compact discs. The capacity could be increased to 15 Gbytes with a suitable violet laser. Despite the tremendous value of a blue laser, advancements have been limited due to a lack of materials which emit blue light or blue-emitting plasmas capable of lasing.

Recombination of injected electrons and holes in InGaN has been extensively pursued as a suitable blue laser [1]. Unfortunately, after over a decade of effort with an estimated expenditure of $1 B, blue diode lasers are still plagued by inadequate substrates, crystal layer dislocations, and defects that increase over time with the requisite high drive currents. Frustration over these and other impediments to commercialization of this important device has given rise to the view that commercial success may depend on the discovery of something completely new [2].

Inverted Lyman and Balmer populations may permit a continuous wave (cw) laser at blue wavelengths. For the last four decades, scientists from academia and industry have been searching for lasers using hydrogen plasma [3-6]. Developed sources that provide a usefully intense hydrogen plasma are high powered lasers, arcs and high voltage DC and RF discharges, synchrotron devices, inductively coupled plasma generators, and magnetically confined plasmas. However, the generation of population inversion is very difficult. Recombining expanding plasma jets formed by methods such as arcs or pulsed discharges is considered one of the most promising methods of realizing an H I laser.

Because the population of hydrogen states is overwhelmingly dominated by the ground state even in the most intense plasmas, the realization of an H I laser requires an overpopulation in a state with $n_i > 2$ which decays to a state with $1 < n < n_i$. Thus, an H I laser based on a Balmer transition is feasible for a mechanism which produces an overpopulation in a corresponding state. The Balmer α, β, γ, and δ lines of atomic hydrogen at 6562.8 Å, 4861.3 Å, 4340.5 Å, 4101.7 Å in the visible region are due to the transitions from $n = 3$, $n = 4$, $n = 5$, and $n = 6$ to $n = 2$, respectively. An H overpopulation of $n > 3$ that is above threshold could be the basis of a blue laser. But, lasing of a blue Balmer line has been difficult to achieve even with cold recombining plasmas. Akatsuka and Suzuki [6], for example, were able to achieve an overpopulation for level pairs 4-3 and 5-4 only for a recombining plasma generated in a arc-heated magnetically trapped expanding plasma jet [6].

Rather than using recombining arcs or recombining electron-hole pairs in semiconductors to achieve lasing at blue wavelengths, a chemical approach was pursued. It was previously reported that a new chemically generated plasma source has been developed that operates by incandescently heating a hydrogen dissociator and a catalyst to provide atomic hydrogen and gaseous catalyst, respectively, which react to produce an energetic plasma called a resonance transfer (rt)-plasma [7-8]. Intense VUV emission was observed at low temperatures (e.g. $\approx 10^3\ K$) and an extraordinary low field strength of about 1-2 V/cm from atomic hydrogen and certain atomized elements or certain gaseous ions which singly or multiply ionize at integer multiples of the potential energy of atomic hydrogen, $E_h = 27.2\ eV$ where E_h is one hartree. The theory has been given previously [9-10].

The ionization of Rb^+ and an electron transfer between two K^+ ions (K^+ / K^+) provide a reaction with a net enthalpy of E_h. The presence of each of these gaseous reactants formed an rt-plasma with atomic hydrogen having strong vacuum ultraviolet (VUV) emission. Remarkably, a stationary inverted Lyman population was also observed, and a collisional radiative model was used to determine that the observed overpopulation was above threshold for $n = 3$ demonstrating that these catalytic reactions may pump a red cw HI laser [11].

For oxygen, there are several chemical reactions that fulfill the catalyst criterion—a chemical or physical process with an enthalpy change equal to an integer multiple of E_h. The bond energy of the oxygen molecule is 5.165 eV, and the first, second, and third ionization energies of an oxygen atom are $13.61806\,eV$, $35.11730\,eV$, and $54.9355\,eV$, respectively [12]. The reactions $O_2 \rightarrow O + O^{2+}$, $O_2 \rightarrow O + O^{3+}$, and $2O \rightarrow 2O^{+}$ provide a net enthalpy of about 2, 4, and 1 times E_h, respectively [12]. Lasing directly from oxygen is unknown, but lasing from inverted water vibration-rotational levels in water plasmas which may be from hydrogen-oxygen mixtures has been achieved several decades earlier [13]. In addition, helium-water plasmas as well as water plasma lasers were explored for a source of submillimeter wavelengths [14]. More recently, emission from OH^* radicals in water and helium-hydrogen water plasmas has been investigated as an efficient source of radiation in the region $\lambda < 2000$ Å for the replacement of expensive working media based on krypton and xenon in microelectronics, photochemistry, and medical applications [15]. These prior water-plasma light sources were based on high-voltage glow discharges.

In our experiments, microwave water plasmas were used as sources of O_2 and atomic hydrogen. The energetic hydrogen atom densities and energies were calculated from the width of the 6563 Å Balmer α line emitted from a control hydrogen and water microwave plasmas. The characteristic emission from the oxygen catalyst was measured. The absolute hydrogen excited state level densities, reduced population densities, and overpopulation densities for lasing were determined from intensity-calibrated high resolution visible spectra in the region 4000 to 7000 Å and VUV spectra in the region 900-1300 Å. Remarkably, stationary inverted Balmer and Lyman populations were observed, and to our knowledge, this is the first report of population inversion in a water plasma. The parameters of a water-plasma laser of Balmer, Paschen, and Brackett series line emission were determined using the spectrally determined reduced population densities. The plasma was further characterized by measuring the electron temperature T_e and density using a Langmuir probe.

The oxygen catalytic reactions may pump a cw HI laser as predicted by a collisional radiative model used to determine that the observed

overpopulation was above threshold. Characteristics of the pumping mechanism and laser power that were consistent with the measured electron temperature, electron density, and reduced population densities were determined from the model.

2. Experimental

The VUV spectrum (900 – 1300 Å), the width of the 6562.8 Å Balmer α line, and the high resolution visible spectra (4000-7000 Å) were recorded on light emitted from microwave, capacitively coupled RF, inductively coupled RF, and glow discharge water plasmas performed according to methods and setups reported previously [8-10, 16-18]. Hydrogen and hydrogen (10%) mixed with xenon, krypton, or nitrogen control plasmas were run under the same conditions. The microwave experimental set up shown in Figure 1 comprised a quartz tube cell, a source of water vapor or ultrapure hydrogen, a flow system, and a visible spectrometer or a VUV spectrometer that was differentially pumped. Water vapor was formed in a heated insulated reservoir and flowed through the half inch diameter quartz tube at a flow rate of 10 standard $cm^3 \cdot s^{-1}$ (sccm) at a corresponding pressure of 50-100 milliTorr. At this pressure, room temperature was sufficient for maintaining the water vapor. The tube was fitted with an Evenson coaxial microwave cavity (Opthos Model #B1) having an E-mode [19-20]. The input power to the plasma at 2.45 GHz by an Opthos model MPG-4M generator was set at 50 W and 90 W as described previously [9-10, 16-18]. The plasma volume was about $10\,cm^3$. Hydrogen control plasma were run under the same conditions. Each gas flow was controlled by a 0-20 sccm range mass flow controller (MKS 1179A21CS1BB) with a readout (MKS type 246). The cell pressure was monitored by a 0-10 Torr MKS Baratron absolute pressure gauge.

In addition, the effect of addition of oxygen or hydrogen to the intensities of the Balmer lines recorded on the water plasma was determined. Using the mass flow controller, 0, 2, 5, 10, and 20 volume % ultrapure gas was mixed with the water vapor while maintaining a constant flow rate and pressure, and each corresponding high resolution visible spectrum (4000-7000 Å) was recorded.

High resolution visible spectra (4000-7000 Å) were recorded on light emitted from hydrogen and water hollow cathode glow discharge plasmas performed according to methods reported previously [16, 18]. The glow discharge cell that comprised a five-way stainless steel cross that served as the anode with a hollow stainless steel cathode. The plasma was generated at the hollow cathode inside the discharge cell. The hollow cathode was constructed of a stainless steel rod inserted into a steel tube, and this assembly was inserted into an Alumina tube. A flange opposite the end of the hollow cathode connected the spectrometer with the cell. It had a small hole that permitted radiation to pass to the spectrometer. An DC power supply (U = 0 - 1 kV, I = 0 - 100 mA) was connected to the hollow cathode to generate a discharge. The DC voltage and current were 300 V and 300 mA, respectively, corresponding to an input power of 90 W. A Swagelok adapter at the very end of the steel cross provided a gas inlet and a connection with the pumping system, and the cell was pumped with a mechanical pump. Valves were between the cell and the mechanical pump, the cell and the monochromator, and the monochromator and its turbo pump. The five-way cross was pressurized with 50-100 milliTorr of gas which was maintained with a gas flow rate of 10 sccm.

High resolution visible spectra (4000-7000 Å) were recorded on light emitted from hydrogen and water capacitively coupled RF discharges plasmas performed according to methods reported previously [16]. The experimental set up comprised a Pyrex cell reactor (38 cm in length and 13 cm ID) with a diode configuration in which the plasma was confined between two parallel circular stainless steel electrodes (0.1 mm thick X 7.6 cm diameter with a 2 cm separation). For spectroscopic measurements on the plasma emission, a 1 cm diameter quartz window was located in the Pyrex cell wall at the center of the gap between the electrodes. At each end of the cell, a Pyrex cap sealed to the cell with a Viton O ring and a C-clamp. One cap incorporated ports for gas inlet and cathode feedthrough. The other cap incorporated ports for gas outlet and anode feedthrough. The cathode was connected to an 13.56 MHz RF generator (RF VII, Inc., Model MN 500) with a matching network (RF Power Products, Inc., Model RF 5S, 300 W). The forward RF power was

90 W, and the reflected power was less than 1 W. The gas flow rate and pressure were 10 sccm and 50-100 milliTorr, respectively.

High resolution visible spectra (4000-7000 Å) were recorded on light emitted from hydrogen and water inductively coupled RF discharges plasmas performed according to methods reported previously [16]. A quartz cell which was 500 mm in length and 50 mm in diameter served as the plasma reactor. A Pyrex cap sealed to the quartz cell with a Viton O ring and a C-clamp incorporated ports for gas inlet, outlet, and photon detection. An unterminated, nine-turn, 17 cm long helical coil (18 gauge magnet wire) wrapped around the outside of the cell was connected to an 13.56 MHz RF generator (RF VII, Inc., Model MN 500) with a matching network (RF Power Products, Inc., Model RF 5S, 300 W). The coil inductance and resistance were $4.7\,\mu H$ and $0.106\,\Omega$, respectively. The coil impedance was $400\,\Omega$ at 13.56 MHz. The forward RF power was 90 W, and the reflected power was less than 1 W. The gas flow rate and pressure were 10 sccm and 50-100 milliTorr, respectively.

The plasma emission was fiber-optically coupled through a 220F matching fiber adapter positioned 2 cm from the cell wall to a high resolution visible spectrometer with a resolution of ± 0.06 Å over the spectral range 1900-8600 Å. The spectrometer was a Jobin Yvon Horiba 1250 M with 2400 groves/mm ion-etched holographic diffraction grating. The entrance and exit slits were set to $20\,\mu m$. The spectrometer was scanned between 6555-6570 Å and 4000-7000 Å using a 0.05 Å step size. The signal was recorded by a PMT with a stand alone high voltage power supply (950 V) and an acquisition controller. The data was obtained in a single accumulation with a 1 second integration time.

The method of Videnovic et al. [21] was used to calculate the energetic hydrogen atom densities and energies from the width of the 6562.8 Å Balmer α line emitted from hydrogen and water microwave plasmas. The full half-width $\Delta\lambda_G$ of each Gaussian results from the Doppler ($\Delta\lambda_D$) and instrumental ($\Delta\lambda_I$) half-widths:

$$\Delta\lambda_G = \sqrt{\Delta\lambda_D^2 + \Delta\lambda_I^2} \qquad (1)$$

$\Delta\lambda_I$ for these experiments was 0.06 Å. The temperature was calculated from the Doppler half-width using the formula:

$$\Delta\lambda_D = 7.16\,X\,10^{-6}\lambda_0\left(\frac{T}{\mu}\right)^{1/2} \text{ (Å)} \qquad (2)$$

where λ_0 is the line wavelength in Å, T is the temperature in K ($1\,eV = 11{,}605\,K$), and μ is the molecular weight (=1 for hydrogen). In each case, the average Doppler half-width that was not appreciably changed with pressure varied by ±5% corresponding to an error in the energy of ±10%. The corresponding number densities for noble gas-hydrogen mixtures varied by ±20%.

To measure the absolute intensity, the high resolution visible spectrometer and detection system were calibrated [22] with 5460.8 Å, 5799.6 Å, and 6965.4 Å light from a Hg-Ar lamp (Ocean Optics, model HG-1) that was calibrated with a NIST certified silicon photodiode. The population density of the $n=3$ hydrogen excited state N_3 was determined from the absolute intensity of the Balmer α (6562.8 Å) line measured using the calibrated spectrometer. The spectrometer response was determined to be approximately flat in the 4000-7000 Å region by ion etching and with a tungsten intensity calibrated lamp. The absolute intensities of $n=4$ to 9 were determined from the absolute intensity of Balmer α ($n=3$) and the relative intensity ratios.

The VUV spectrometer was a normal incidence 0.2 meter monochromator equipped with a 1200 lines/mm holographic grating with a platinum coating that covered the region 20 – 5600 Å. The VUV spectrum was recorded with a CEM. The wavelength resolution was about 0.2 Å (FWHM) with slit widths of $50\,\mu m$. The increment was 2 Å and the dwell time was $500\,ms$. The VUV spectra (900 – 1300 Å) of the water and control hydrogen plasmas were recorded at 90 W input power.

The spectrometer was calibrated between 400-2000 Å with a standard discharge light source using He, Ne, Ar, Kr, and Xe lines: He I (584 Å), He II (304 Å), Ne I (735 Å), Ne II (460.7 Å), Ar I (1048 Å), Ar II (932 Å), Kr II (964 Å), Xe I (1295.6 Å), Xe II (1041.3 Å), Xe II (1100.43 Å). The wavelength and intensity ratios matched those given by NIST [23]. The spectrometer response was determined to be approximately flat in the 1000-1300 Å region. The calculation of the number density of the $n=3$ to 9 states was corrected for the minor variation of the sensitivity with wavelength in this region.

The electron density and temperature of the rt-plasma was determined using a compensated Langmuir probe according to the method given previously [24].

3. Results and discussion

A. Hydrogen Balmer and Lyman series emission

The high resolution visible spectra (4000-6700 Å) of the cell emission from a hydrogen microwave plasma with 90 W input power, a water microwave plasma with 50 W input power, and a water microwave plasma with 90 W input power are shown in Figures 2-4, respectively. As shown by the absolute intensity measurements of the Balmer lines of the hydrogen microwave plasma, we observed the known ratios of the Balmer lines. In contrast, the population of the levels $n=4$, $n=5$, and $n=6$ of hydrogen were continuously inverted with respect to $n=3$ in the water plasma spectrum shown in Figure 3. The relative intensities of the Balmer lines of microwave plasmas of hydrogen (90-2%) mixed with xenon, krypton, or nitrogen at 50 W were equivalent to those of hydrogen alone; thus, the inversion is not inherent to a hydrogen plasma generated by microwaves. As shown in Figure 4, when the input power was increased to 90 W, the $n=5$ and $n=6$ levels were further continuously inverted with respect to $n=4$. The levels $n=7$, $n=8$, and $n=9$ of hydrogen were also continuously inverted with respect to $n=3$. Thus, wavelength tunebility may be achieved by varying the microwave power with lasing between the corresponding power-dependent inverted levels. The requirement for a stoichiometric mixture was fairly exacting since it was observed that additions of increasing partial pressures of pure hydrogen or oxygen progressively reversed the inversion at a mole fraction over the stoichiometric ratio of greater than 2%.

The VUV spectra (900 – 1300 Å) of the cell emission from hydrogen microwave and the water microwave plasmas with 90 W input power are shown in Figure 5. An inverted Lyman population was also observed from the water plasma emission with the inversion observed in the visible as shown in Figure 2 extending to the $n=2$ level. No inversion was observed for the hydrogen microwave plasma.

No inversion was observed with inductively or capacitively RF driven or high voltage glow discharge water plasmas as shown in Figures 6-8, respectively. However, intense emission of OH^* radicals in water plasmas was observed from glow discharge as well as microwave sources

as shown in Figures 8 and 4, respectively. As discussed previously, the glow discharge plasma has been extensively studied as a light source based on the emission of OH^* radicals [15]. Shuaibov et al. [25] give the spectrum of a glow discharge of a He/H_2O mixture and assign the $OH(A-X)$ emission. As a comparison, the $OH(A-X)$ microwave water plasma emission spectrum in the region of 2800-3300 Å is given in Figure 9. The (1-0) R-branch and the (1-0) Q-branch are observed in the 2800-2950 Å region as shown in Figure 10. The (0-0) R-branch and the (0-0), (1-1), and (2-2) Q-branches are observed in the 3000-3300 Å region as shown in Figure 11.

We had shown previously that the conditions of the particular discharge may be a major parameter in the observation of excessive Doppler Balmer line broadening with plasmas of hydrogen and a noble ion having an ionization potential of an integer multiple of E_h [8-11, 16-18]. We proposed that the corresponding energetic hydrogen formed with an Evenson microwave cavity may be a means to achieve population inversion.

Other explanations of the population inversion were ruled out. The spectrometer response was determined to be approximately flat in the 4000-7000 Å region by ion etching and with an intensity calibrated lamp. Furthermore, the Balmer and Lyman line intensity ratios of the control hydrogen plasmas closely matched those obtained using the NIST Einstein A coefficients [23]. Since these ratios did not change as the pressure was lowered, and the hydrogen pressure was lower in the water plasma than the control, the NIST Einstein A coefficients were used to calculate the number density ratios from the water plasma emission.

To determine the optical thickness of the water plasmas of this study, $\tau_\omega(L)$, the effective path length at a given frequency ω, was calculated using

$$\tau_\omega(L) = \kappa_\omega L \tag{3}$$

where L is the path length and κ_ω is the absorption coefficient given by

$$\kappa_\omega = \sigma_\omega X N_H \tag{4}$$

where σ_ω is the absorption cross section and N_H is the number density of the absorber. For optically thin plasmas $\tau_\omega(L) < 1$, and for optically thick plasmas $\tau_\omega(L) > 1$. By orders of magnitude, self absorption of Lyman emission by $n=1$ state hydrogen dominates since $n=1$ H dominates the H

population distribution. At 1215.67 Å, the effective path length $\tau_\omega(5\,cm)$ was calculated from Eq. (3) using the absorption cross section for Lyman α emission, $\sigma = 4\,X\,10^{-16}\,cm^2$ [26], and $N_H = 6\,X\,10^{13}\,cm^{-3}$.

$$\tau_\omega(5\,cm) = \kappa_\omega L = \left(4\,X\,10^{-16}\,cm^2\right)\left(6\,X\,10^{13}\,cm^{-3}\right)(5\,cm) = 1\,X\,10^{-1} \qquad (5)$$

Since $\tau_\omega(5) << 1$, the water plasmas were optically thin. Furthermore, the water plasmas were determined to be optically thin for hydrogen absorption of the Balmer and as well as the additional Lyman lines. Thus, absorption of 6562.8 Å and 4861.3 Å and 1215.67 Å emission by $n = 2$ and $n = 1$ state atomic hydrogen, respectively, may be neglected as the cause of the inverted ratios.

The absorption cross section of Balmer emission by water is insignificant—nine orders of magnitude less than in the Lyman region [27]. Thus, the Balmer lines were used to determine the over populations in Table 1, except for the $n = 2$ level which was determined from the intensities of the Lyman lines. The effective path length $\tau_\omega(5\,cm)$ was calculated from Eq. (3) using the absorption cross section of water for Lyman α emission, $\sigma = 1.6\,X\,10^{-17}\,cm^2$ [28], and the water number density, $N_{H_2O} = 2.5\,X\,10^{15}\,cm^{-3}$, calculated from the measured pressure. Thus, $\tau_\omega(5\,cm)$ is given by

$$\tau_\omega(5\,cm) = \kappa_\omega L = \left(1.6\,X\,10^{-17}\,cm^2\right)\left(2.5\,X\,10^{15}\,cm^{-3}\right)(5\,cm) = 0.2 \qquad (6)$$

Since $\tau_\omega(5) < 1$, the water plasmas were optically thin for Lyman α emission.

B. Measurement of hydrogen atom temperature and number density from Balmer line broadening

To further characterize the water plasma, the width of the 6562.8 Å Balmer α line ($n = 3$ to $n = 2$) was measured on light emitted from the microwave discharges of pure hydrogen alone and water vapor maintained under equivalent conditions using the high resolution visible spectrometer as shown in Figures 12 and 13, respectively. The method of Videnovic et al. [21] was used to calculate the hydrogen atom energies and densities from the line width. Significant line broadening of 55 eV and an atom density of $6\,X\,10^{13}\,atoms/cm^3$ was observed from the water plasma compared to an average hydrogen atom temperature of 1 eV and a density of $6\,X\,10^{11}\,atoms/cm^3$ for hydrogen alone. Similarly, using a

Langmuir probe as described previously [24], the electron temperature T_e measured on the microwave water plasmas was higher, 2.0 eV, compared to the $T_e \leq 1\,eV$ measured on the hydrogen plasma at the same 50 W input power.

We have assumed that Doppler broadening due to thermal motion was the dominant source in the water plasmas to the extent that other sources may be neglected. To confirm this assumption, each source is now considered. In general, the experimental profile is a convolution of a Doppler profile, an instrumental profile, the natural (lifetime) profile, Stark profiles, van der Waal's profiles, a resonance profile, and fine structure. The instrumental half-width is measured to be ±0.06 Å. The natural half-width of the Balmer α line given by Djurovic and Roberts [29] is $1.4\,X\,10^{-3}$ Å which is negligible. The fine structure splitting is also negligible.

Stark broadening of hydrogen lines in plasmas can not be measured at low electron densities using conventional emission or absorption spectroscopy because it is hidden by Doppler broadening. In the case of the Lyman α line, the Stark width exceeds the Doppler width only at $n_e > 10^{17}\,cm^{-3}$ for temperatures of about 10^4 K [30].

The relationship between the Stark broadening $\Delta\lambda_S$ of the Balmer β line in nm, the electron density n_e in m^{-3}, and the electron temperature T_e in K is

$$\log n_e = C_0 + C_1 \log(\Delta\lambda_S) + C_2[\log(\Delta\lambda_S)]^2 + C_3 \log(T_e) \qquad (7)$$

where $C_0 = 22.578$, $C_1 = 1.478$, $C_2 = -0.144$, and $C_3 = 0.1265$ [31]. From Eq. (7), to get a Stark broadening of only 1 Å with $T_e = 9000\,K$, an electron density of about $n_e \sim 3\,X\,10^{15}\,cm^{-3}$ is required compared to that of the water plasma of $n_e \doteq 0.2\,X\,10^{8}\,cm^{-3}$ determined using a Langmuir probe, over seven orders of magnitude less. Gigosos and Cardenoso [32] give the observed Balmer α Stark broadening for plasmas of hydrogen with helium or argon as a function of the electron temperature and density. For example, the Stark broadening of the Balmer α line recorded on a $H + He^+$ plasma is only 0.33 Å with $T_e = 20{,}000\,K$ and $n_e = 1.4\,X\,10^{14}\,cm^{-3}$. Thus, the Stark broadening was also insignificant.

The statistical curve fit of the hydrogen and water microwave plasma emission are shown in Figures 12 and 13, respectively. In each case, the data matched a Gaussian profile having the X^2 and R^2 values

given in Figures 12 and 13. The absence of Stark broadening in the water plasma is also evident by the good fit to a Gaussian profile rather than a Voigt profile as shown in Figure 13.

A linear Stark effect arises from an applied electric field that splits the energy level with principal quantum number n into $(2n-1)$ equidistant sublevels. The magnitude of this effect given by Videnovic et al. [21] is about $2\,X\,10^{-2}\ nm/kV\cdot cm^{-1}$. No applied electric field was present in our study; thus, the linear Stark effect should be negligible.

The plasma was evaluated for optical thickness. The absorption cross section for Balmer α emission is $\sigma = 1\,X\,10^{-16}\ cm^2$ [26]. As discussed *infra.*, an estimate based on Lyman line intensity, the $n=2$ H atom density is $\sim 1.39\,X\,10^{9}\ cm^{-3}$. Thus, for a plasma length of $5\ cm$, the effective path length, $\tau_\omega(5\ cm)$, calculated from Eq. (3) for Balmer α is

$$\tau_\omega(5\ cm) = \kappa_\omega L = \left(1\,X\,10^{-16}\ cm^2\right)\left(1.39\,X\,10^{9}\ cm^{-3}\right)(5\ cm) = 6.95\,X\,10^{-7} \qquad (8)$$

Since $\tau_\omega(5) <<< 1$, the water plasmas were optically thin; thus, the self absorption of 6562.8 Å emission by $n=2$ state atomic hydrogen may be neglected as a source of the observed broadening.

As discussed above, an estimate based on emission line profiles places the total H atom density of the water plasma at $\sim 6\,X\,10^{13}\ cm^{-3}$. Since this is overwhelmingly dominated by the ground state, $N_H = 6\,X\,10^{13}\ cm^{-3}$ will be used. Usually, the atomic hydrogen collisional cross section in plasmas is on the order of $10^{-18}\ cm^2$ [33]. Thus, for $N_H = 6\,X\,10^{13}\ cm^{-3}$, collisional or pressure broadening is negligible.

Prior studies that reported fast H, attributed the observation to acceleration of ions in a high electric fields at the cathode fall region and an external field Stark effect [21, 34-35]. Observations with a microwave plasma having no high DC field present was reported previously [16-18]. Microwave helium-hydrogen and argon-hydrogen plasmas showed extraordinary broadening corresponding to an average hydrogen atom temperature of $180\text{-}210\ eV$ and $110\text{-}130\ eV$, respectively. Whereas, pure hydrogen and xenon-hydrogen microwave plasmas showed no excessive broadening corresponding to an average hydrogen atom temperature of $<2\ eV$ [16-18]. The formation of fast H was explained by a resonance energy transfer between hydrogen atoms and Ar^+ or He^+ of an integer multiple of the potential energy of atomic hydrogen, $27.2\ eV$.

As in the case of the argon-hydrogen or helium-hydrogen plasmas, no hydrogen species, H^+, H_2^+, H_3^+, H^-, H, or H_2, of the water plasmas responds to the microwave field; rather, only the electrons respond. However, the measured electron temperature in these microwave plasmas was about 1-2 eV; whereas, the measured neutral hydrogen temperature was much higher, 55 eV. This requires that $T_i >> T_e$ which can not be due to direct ion coupling to the microwave power or electron-collisional heating. Nor, can this result be explained by electric field acceleration of charged species as proposed for glow discharges [21, 34-35] since in microwave driven plasmas, there is no high electric field in a cathode fall region ($>1\ kV/cm$) to accelerate positive ions. The observation of excessive Balmer line broadening in a microwave driven plasma requires a source of energy. In the case of the water plasma, we propose that the source is the energy is due to a resonant energy transfer between hydrogen atoms and oxygen. The catalysis mechanism was supported by the observation of O^{2+} at 3715.0 Å, 3754.8 Å, and 3791.28 Å as shown in Figure 14 as well as the extraordinary Balmer line broadening of 55 eV compared to 1 eV for hydrogen alone. This energy may further be the basis of the pumping source for the observed population inversions.

Then the inverted population is explained by a resonance energy transfer between hydrogen and oxygen to yield fast $H(n=1)$ atoms. The emission of excited state H from fast $H(n=1)$ atoms excited by collisions with the background H_2 has been discussed by Radovanov et al. [35]. Collisions with oxygen may also play a role in the inversion since inverted hydrogen populations are observed in the case of alkali nitrates [11] and water vapor plasmas. Formation of H^+ is also predicted by a collisional radiative model [11] which is far from thermal equilibrium in terms of the hydrogen atom temperature. Akatsuka et al. [6] show that it is characteristic of cold recombining plasmas to have the high lying levels in local thermodynamic equilibrium (LTE); whereas, population inversion is obtained when T_e suddenly decreases concomitant with rapid decay of the lower lying states.

C. Observed Level Population and Lasing Ability

To determine the potential of the water-plasma as a laser medium, the absolute reduced Balmer population density of the excited hydrogen atoms $\frac{N_n}{g_n}$ with principal quantum numbers $n=1$ to 9 were obtained from N, their absolute intensity integrated over the visible spectral peaks shown in Figures 3 and 4 corrected by their Einstein coefficients, divided by g, the statistical weight ($g=2n^2$), as discussed by Akatsuka et al. [6]. As shown in Table 1, $\frac{N_n}{g_n}$ for quantum number $n=3,4,5,6$ recorded on a water microwave plasma at 90 W input was determined to be $3.44\,X\,10^8 cm^{-3}$, $3.44\,X\,10^8 cm^{-3}$, $9.02\,X\,10^8 cm^{-3}$, and $385\,X\,10^8 cm^{-3}$, respectively.

The population of the $n=2$ level was determined from the VUV spectrum (900 – 1300 Å) of the microwave water plasma shown in Figure 5. From the number densities of the levels determined from the absolute Balmer line intensities given in Table 1 and the Lyman lines intensities shown in Figure 5, it was found that

$$\frac{N_4}{N_3}\text{Balmer} = 4.66;\ \frac{N_4}{N_3}\text{Lyman} = 4.46 \qquad (9)$$

Since $\frac{N_4}{N_3}$ determined from the Lyman series and the Balmer series was about the same, and the Balmer α line was absolutely measured, the absolute number density for $n=2$ given in Table 1 was determined from the absolute Balmer α line intensity.

$$(N_2)_{\text{Balmer}} = (N_3)_{\text{Balmer}} \times \left(\frac{(N_2)Lyman}{(N_3)Lyman}\right) \qquad (10)$$

Using $N_3 = 6.20\,X\,10^9\,cm^{-3}$ and $g_2 = 8$, $\frac{N_2}{g_2}$ was determined to be $1.74\,X\,10^8\,cm^{-3}$.

With appropriate cavity length and mirror reflection coefficient, cw laser oscillations may be obtained between states having an overpopulation ratio determined by $\frac{N_i}{N_f}\frac{g_f}{g_i} > 1$ as shown in Table 1 where i represents the quantum number of the initial state and f represents that of the final state [6]. On this basis, it was determined that lasing is possible over a wide range from far infrared to violet wavelengths. Representative transitions and wavelengths are shown in Table 2. The important parameter for lasing is that the reduced overpopulation density is above threshold. Using standard laser cavity equations [6], it

was determined that the threshold condition is achievable with micron to submillimeter laser cavities for several commercially important wavelengths emitted from these plasmas. For plasma properties of this experiment determined using a Langmuir probe ($T_e = 2.0\,eV$, electron density $n_e = 0.2\,X\,10^8\,cm^{-3}$), conditions for lasing at 12,818.1 Å, 4340.5 Å, and 4101.7 Å corresponding to the transitions $5 \rightarrow 3$, $5 \rightarrow 2$, and $6 \rightarrow 2$, respectively, were determined assuming a cavity length of 100 cm and a combined mirror reflection coefficient of 0.99, as given in Table 3. The overpopulation ratios $\frac{N_5}{N_3}\frac{g_3}{g_5}$, $\frac{N_5}{N_2}\frac{g_2}{g_5}$, and $\frac{N_6}{N_2}\frac{g_2}{g_6}$ given in Table 1 were 112, 221, and 67, respectively. Threshold reduced $n = 5$ overpopulation densities of about $0.49\,X\,10^7\,cm^{-3}$ and $4.6\,X\,10^7\,cm^{-3}$ are required for lasing to $n = 3$ and $n = 2$, respectively, and, a corresponding threshold reduced $n = 6$ overpopulation density of $6.9\,X\,10^7\,cm^{-3}$ is required for lasing to $n = 2$. The actual reduced overpopulation densities were much greater, $3.8\,X\,10^{10}\,cm^{-3}$, $3.8\,X\,10^{10}\,cm^{-3}$, and $1.2\,X\,10^{10}\,cm^{-3}$, respectively. Thus, lasing may be possible with cavity lengths as small as 0.01 cm, 0.2 cm, and 0.6 cm, respectively.

D. Level Population Model and Inversion Pumping

In order to estimate hydrogen excited state level populations and inversion pumping, the collisional radiative model [6, 36] is applied to the plasma conditions obtained herein ($T_e \sim 0.8\,eV$, $n_e \sim 10^9\,cm^{-3}$). The collisional radiative model explicitly includes all level population and de-population mechanisms for each excited level from every other excited level in the hydrogen atom. Excited level n is, then, populated by collisional excitation from all lower excited states, and collisional and radiative de-excitation from all higher excited states. De-population explicitly includes collisional and radiative de-excitation to all lower states, and collisional excitation to all higher levels. Independent ionization loss, radiative recombination, and dielectronic recombination are included for all levels as well. A separate balance equation is prescribed for each individual level and is coupled to all other level equations through the population and de-population terms described above.

In order to close the set of equations, truncation was chosen at $n = 9$. This is justified by both the experimental observation of no measurable emission from higher lying states and *a posteriori* via the model results

indicating a progression of negligibly small level densities beyond $n=6$. The ground state ($n=1$) level population cannot be determined by this method since the important affects of dissociation, molecular recombination, and transport are not included. As discussed earlier (Sec. 3A), however, an estimate based on emission line profiles places the total H atom density $\sim 6\,X\,10^{13}\,cm^{-3}$. Since this is overwhelmingly dominated by the ground state, the assignment $N_1 = 6\,X\,10^{13}\,cm^{-3}$ will be made throughout.

Solution to the $n=2$ to 9 level equations under these conditions shows no inversion in any of the level populations. This is an expected result for a steady, thermal plasma. Also, as expected, the dominant mechanisms are found to be population by collisional excitation and de-population by radiative decay.

The results of this calculation are inconsistent with the spectroscopic observations. Absolutely calibrating the monochromator for the Balmer lines however yields, $N_{3-8} > 10^9\,cm^{-3}$ as shown in Table 1. There is, then, a heretofore undetermined mechanism providing direct excited state population, *i.e.* pumping. To help quantify the affects of this mechanism, the level equations are once again evaluated with $N_{5,6}$ fixed to the values given in Table 1 and the inclusion of independent pumping rates for $n=5$ and 6. Since spectroscopic results indicate $n=3$ to 8 inversion, pumping is prescribed to the $n=5$ and 6 states from the ground state, $n=1$. The results from this calculation for $n=1$ to 9 are summarized in Table 4.

Now collisional mechanisms from the $n=5$ and 6 states as well as ground state collisional excitation and radiative decay significantly contribute to population and de-population rates. In addition, demonstrated inversion in the populations with the possibility of laser transitions from i) $n=3$, $n=4$, $n=5$, $n=6$, and $n=7$ to $n=2$, ii) $n=4$, $n=5$, and $n=6$ to $n=3$ and iii) $n=5$ and $n=6$ to $n=4$ are predicted.

The pumping rates and corresponding powers were also determined in this analysis yielding the rates given in Table 5. For example, in order for the $n=5$ state to be pumped to the desired level, the pumping mechanism must represent a transition rate density of $8.4\,X\,10^{19}\,cm^{-3}\cdot s^{-1}$ from $n=1$ to $n=5$. Since the $n=5$ state has a excitation energy of $13.05\,eV$, this pumping mechanism consumes energy at a rate of $\sim 175.3\,W\cdot cm^{-3}$. Since this plasma is in the steady state, energy

consumption at this rate implies an equivalent production at the same rate .which is returned as H radiation corresponding to transitions to $n<5$. No other source of power was evident except the that proposed due to the catalytic reaction of oxygen with hydrogen.

E. Blue and infrared Laser applications

A micro-water laser may possible using proven approaches. As an advancement to the liquid based predecessor, micro-organic dye lasers have been developed by suspending each dye molecule in a cavity of a zeolite rather than in solution [36]. If they can be electrically pumped, such devices may eventually be competitive with semiconductor diode lasers; however, currently they require optical pumping. Microwaves are transparent to materials comprised of silicon or aluminum oxides. Thus, microcavities containing water vapor could potentially provide more competitive alternative microlasers for microelectronics applications that do not suffer from lattice constant and thermal expansion coefficient incompatibilities or require sophisticated materials or structures such as multiple quantum wells [37-38].

Lasing is possible at blue wavelengths which are ideal for many communications and microelectronics applications as well as at a wavelength of 1.3 μm which is ideal for transmission through glass optical fibers. The emission wavelength of the potential water laser is about 400 nm which is suitable for the next generation 15-Gbyte DVDs [1]. Currently, the ideal laser diode for telecommunications applications is the $In_xGa_{1-x}As_yP_{1-y}$ diode laser wherein a lattice constant mismatch requires that the laser be separate from the silicon circuits. An integrated laser would revolutionize telecommunications, electronics, and computing [39]. Conceptually, we see no obvious impediment to integration of a water-plasma laser. In addition, many more laser wavelengths corresponding to Balmer, Paschen, and Brackett lines are possible. With the capability of lasing over the widest range of atomic wavelengths of any known atomic laser, far infrared to violet, the hydrogen laser based on water-plasma may prove to be the most versatile laser yet discovered.

The observed $175\ W \cdot cm^{-3}$ pumping power of the $n=5$ state is unprecedented given the microwave input power of $\sim 9\ W \cdot cm^{-3}$. Using the

model, the corresponding lasing power and efficiency of the 5-2 transition are high, $5\,W \cdot cm^{-3}$ and 56%, respectively, compared to the highest power commercially available for a He/Ne laser of about 50 mW at 0.01% efficiency. Our results indicate that with a microwave input power of 1 kW, 1000 cm^3 of water vapor plasma medium is capable of 5 kW cw laser power, comparable to the most powerful industrial cutting and welding lasers at about 50 times the efficiency. This obviously changes the prospects for many laser applications that have been limited by size or power requirements such as space-based lasers [40] and the National Ignition Facility (NIF) [41].

An even more significant opportunity exists for electric power generation. Light-weigh, compact traveling-wave-tube microwave power sources that are ubiquitous in applications such as microwave ovens are about 95% efficient and are extremely inexpensive (900 W unit is about $11). In addition, conversion of monochromatic spontaneous and/or stimulated emission from the water plasma cell to electricity using a photovoltaic with a band gap that is matched to the wavelength can be achieved with greater than 80% efficiency at a photovoltaic cell irradiation up to $1000\,W \cdot cm^{-2}$ (7300 suns equivalent) requiring less than 1/7300 the PV active area of solar conversion [42-45]. Given that ultra-light, thin film photovoltaics are mass-produced at about $\sim 1¢\,cm^{-2}$, we propose a competitive direct electric power generation system comprising an open cavity microwave driven water plasma surrounded by a photovoltaic converter, both placed inside a vacuum vessel. This design eliminates the need for a window since the results of the model indicate that over 90% of the $200\,W \cdot cm^{-3}$ of optical power (total $n = 1 \rightarrow 5,6$ pumping power given in Table 5) due to catalysis involves Lyman emission. For short wavelength radiation, the quantum efficiency may be significantly greater than one which compensates for the photon-band-gap energy mismatch [46]. Using current technology, plasma cell power densities comparable to those of an internal combustion engine (ICE) and the efficient direct conversion of the power into electricity may be realizable with a system having reduced weight, capital cost, infrastructure requirements, and environmental impact than the ICE. Furthermore, this technology is sustainable; whereas, the ICE is not.

4. Conclusion

The reactions O_2 to O and O^{2+}, O_2 to O and O^{3+}, and $2O$ to $2O^{+}$ provide a net enthalpy of an integer multiple of the potential energy of atomic hydrogen of 2, 4, and 1 times $27.2\,eV$, respectively. Stationary inverted H Balmer and Lyman populations were observed from a low pressure water-vapor microwave discharge plasmas. The ionization and population of excited atomic hydrogen levels was attributed to energy provided by the catalytic resonance energy transfer between hydrogen atoms and molecular oxygen formed in the water plasma. The catalysis mechanism was supported by the observation of O^{2+} and H Balmer line broadening of 55 eV compared to 1 eV for hydrogen alone. The catalysis reaction, and consequently the inversion, depended on specific plasma conditions provided by the Evenson microwave cavity. In contrast, no inversion was observed using RF or glow discharge cells. In addition, the requirement for the natural hydrogen-oxygen stoichiometry of the water plasma was stringent in that a deviation by over 2% excess of either gas caused a reversal of the inversion.

The high hydrogen atom temperature with a relatively low electron temperature, $T_e = 2\,eV$, due to the catalysis reaction were characteristic of cold recombining plasmas. These conditions of a water plasma favored an inverted population in the lower levels. Thus, the catalysis of atomic hydrogen may pump a cw HI laser with expected laser oscillations from i) $n=3$, $n=4$, $n=5$, $n=6$, $n=7$ and $n=8$ to $n=2$, ii) $n=4$, $n=5$, $n=6$, and $n=7$ to $n=3$ and iii) $n=5$ and $n=6$ to $n=4$. A micro-water laser capable of integration may possible using proven approaches. Many more laser wavelengths corresponding to Balmer, Paschen, and Brackett lines are possible. With the capability of lasing over the widest range of atomic wavelengths of any known atomic laser, far infrared to violet, the hydrogen laser based on water-plasma may prove to be the most versatile laser yet discovered.

With the development of a pumping power of over $200\,W\cdot cm^{-3}$ for a microwave input power of $\sim 9\,W\cdot cm^{-3}$, new opportunities are possible for laser applications that are limited by power and/or size considerations. In addition, a potential revolutionary application is the direct generation of electrical power using photovoltaic conversion of the spontaneous or stimulated water vapor plasma emission.

References

1. S. Nakamura, "The roles of structural imperfections in InGaN-based blue light-emitting diodes and laser diodes, Science, Vol. 281, (1998), pp. 956-962.
2. R. W. Hardin, "Challenges remain for blue diode lasers", OE Reports, SPIE, No. 192, Dec. (1999), http://www.spie.org/web/oer/december/dec99/cover1.html.
3. L. I. Gudzenko, L. A. Shelepin, Sov. Phys. JETP, Vol. 18, (1963), p. 998.
4. S. Suckewer, H. Fishman, J. Appl. Phys., Vol. 51, (1980), p. 1922.
5. W. T. Silfvast, O. R. Wood, J. Opt. Soc. Am. B, Vol. 4, (1987), p. 609.
6. H. Akatsuka, M. Suzuki, "Stationary population inversion of hydrogen in arc-heated magnetically trapped expanding hydrogen-helium plasma jet", Phys. Rev. E, Vol. 49, (1994), pp. 1534-1544.
7. R. Mills, J. Dong, Y. Lu, "Observation of Extreme Ultraviolet Hydrogen Emission from Incandescently Heated Hydrogen Gas with Certain Catalysts", Int. J. Hydrogen Energy, Vol. 25, (2000), pp. 919-943.
8. R. Mills and M. Nansteel, P. Ray, "Argon-Hydrogen-Strontium Discharge Light Source", IEEE Transactions on Plasma Science, in press.
9. R. L. Mills, P. Ray, B. Dhandapani, M. Nansteel, X. Chen, J. He, "Spectroscopic Identification of Transitions of Fractional Rydberg States of Atomic Hydrogen", J. of Quantitative Spectroscopy and Radiative Transfer, in press.
10. R. L. Mills, P. Ray, B. Dhandapani, M. Nansteel, X. Chen, J. He, "New Power Source from Fractional Quantum Energy Levels of Atomic Hydrogen that Surpasses Internal Combustion", J Mol. Struct., in press.
11. R. Mills, P. Ray, R. M. Mayo, "Chemically-Generated Stationary Inverted Lyman Population for a CW HI Laser", J Vac. Sci. and Tech. A, submitted.
12. D. R. Linde, CRC Handbook of Chemistry and Physics, 79 th Edition, CRC Press, Boca Raton, Florida, (1998-1999), p. 9-55 and p. 10-175.
13. A., Crocker, H. A. Gebbie, M. F. Kimmitt, L. E. S. Mathias, "Stimulated emission in the far infra-red", Nature, Vol. 201, (1964), pp. 250-251.
14. W. J. Sarjeant, Z. Kucerovsky, E. Brannen, "Excitation processes and relaxation rates in the pulsed water vapor laser", Applied Optics, Vol. 11, No. 4, (1972), pp. 735-741.

15. A. K. Shuaibov, A. I. Dashchenko, I. V. Shevera, "Stationary radiator in the 130-190 nm range based on water vapour plasma", Quantum Electronics, Vol. 31, No. 6, (2001), pp. 547-548.
16. R. L. Mills, P. Ray, E. Dayalan, B. Dhandapani, J. He, "Comparison of Excessive Balmer α Line Broadening of Inductively and Capacitively Coupled RF, Microwave, and Glow Discharge Hydrogen Plasmas with Certain Catalysts", IEEE Transactions on Plasma Science, submitted.
17. R. L. Mills, P. Ray, "Substantial Changes in the Characteristics of a Microwave Plasma Due to Combining Argon and Hydrogen", New Journal of Physics, www.njp.org, Vol. 4, (2002), pp. 22.1-22.17.
18. R. L. Mills, P. Ray, B. Dhandapani, J. He, "Comparison of Excessive Balmer α Line Broadening of Glow Discharge and Microwave Hydrogen Plasmas with Certain Catalysts", J. of Applied Physics, submitted.
19. F. C. Fehsenfeld, K. M. Evenson, H. P. Broida, "Microwave discharges operating at 2450 MHz", Review of scientific Instruments, Vol. 35, No. 3, (1965), pp. 294-298.
20. B. McCarroll, "An improved microwave discharge cavity for 2450 MHz", Review of Scientific Instruments, Vol. 41, (1970), p. 279.
21. I. R. Videnovic, N. Konjevic, M. M. Kuraica, "Spectroscopic investigations of a cathode fall region of the Grimm-type glow discharge", Spectrochimica Acta, Part B, Vol. 51, (1996), pp. 1707-1731.
22. J. Tadic, I. Juranic, G. K. Moortgat, "Pressure dependence of the photooxidation of selected carbonyl compounds in air: n-butanal and n-pentanal", J. Photochemistry and Photobiology A: Chemistry, Vol. 143, (2000), 169-179.
23. NIST Atomic Spectra Database, www.physics.nist.gov/cgi-bin/AtData/display.ksh.
24. D. Barton, J. W. Bradley, D. A. Steele, and R. D. Short, "Investigating radio frequency plasmas used for the modification of polymer surfaces," J. Phys. Chem. B, Vol. 103, (1999), pp. 4423-4430.
25. A. K. Shuaibov, L. L. Shimon, A. I. Dashchenko, I. V. Shevera, "Optical characteristics of a glow discharge in a He/H_2O mixture", Plasma Physics Reports, Vol. 27, No. 10, (2001), pp. 897-900.
26. H. Okabe, *Photochemistry of Small Molecules*, John Wiley & Sons, New York, (1978).

27. J. G. Calvert, J. N. Pitts, *Photochemistry*, John Wiley & Sons, New York, (1966), pp. 200-202.
28. R. K. Vatsa, H. R. Volpp, "Absorption cross-section for atmospheric important molecules at the H atom Lyman α wavelength (121.567 nm)", Chemical Physics Letters, Vol. 340, (2001), pp. 289-295.
29. S. Djurovic, J. R. Roberts, "Hydrogen Balmer alpha line shapes for hydrogen-argon mixtures in a low-pressure rf discharge", J. Appl. Phys., Vol. 74, No. 11, (1993), pp. 6558-6565.
30. J. Seidel, "Theory of two-photon polarization spectroscopy of plasma-broadened hydrogen L_α line", Phys. Rev. Letts., Vol. 57, No. 17, (1986), p. 2154.
31. A. Czernikowski, J. Chapelle, Acta Phys. Pol. A., Vol. 63, (1983), p. 67.
32. M. A. Gigosos, V. Cardenoso, "New plasma diagnosis tables of hydrogen Stark broadening including ion dynamics", J. Phys. B: At. Mol. Opt. Phys., Vol. 29, (1996), pp. 4795-4838.
33. A. Corney, Atomic and Laser Spectroscopy, Clarendon Press, Oxford, (1977).
34. M. Kuraica, N. Konjevic, "Line shapes of atomic hydrogen in a plane-cathode abnormal glow discharge", Physical Review A, Volume 46, No. 7, October (1992), pp. 4429-4432.
35. S. B. Radovanov, K. Dzierzega, J. R. Roberts, J. K. Olthoff, "Time-resolved Balmer-alpha emission from fast hydrogen atoms in low pressure, radio-frequency discharges in hydrogen", Appl. Phys. Letts., Vol. 66, No. 20, (1995), pp. 2637-2639.
36. S. R. Forrest, "Solid-state lasers: Lasing from a molecular sieve", Nature Vol. 397, (1999), pp. 294-295.
37. T. Someya, R. Werner, A. Forchel, M. Catalano, R. Cingolani, Y. Arakawa, "Room temperature lasing at blue wavelengths in gallium nitride microcavities", Science, Vol. 285, (1999), pp. 1905-1906.
38. S. Nakamura, "The roles of structural imperfections in InGaN-based blue light-emitting diodes and laser diodes, Science, Vol. 281, pp. 956-962.
39. P. Ball, "Let there be light", Nature, Vol. 409, (2001), pp. 974-976.
40. http://www.airbornelaser.com; http://home.achilles.net/~jtalbot/history/starwars.html; http://www.peacevision.org.uk/papers/webb.html.

41. R. L. McCrory, et al., "OMEGA ICF experiments and preparation for direct drive ignition on NIF", Nuclear Fusion, Vol. 41, No. 10, (2001), pp. 1414-1422.
42. L. C. Olsen, D. A. Huber, G. Dunham, F. W. Addis, "High efficiency monochromatic GaAs solar cells", in *Conf. Rec. 22nd IEEE Photovoltaic Specialists Conf.*, Las Vegas, NV, Vol. I, Oct. (1991), pp. 419-424.
43. R. A. Lowe, G. A. Landis, P. Jenkins, "Response of photovoltaic cells to pulsed laser illumination", IEEE Transactions on Electron Devices, Vol. 42, No. 4, (1995), pp. 744-751.
44. R. K. Jain, G. A. Landis, "Transient response of gallium arsenide and silicon solar cells under laser pulse", Solid-State Electronics, Vol. 4, No. 11, (1998), pp. 1981-1983.
45. P. A. Iles, "Non-solar photovoltaic cells", in *Conf. Rec. 21st IEEE Photovoltaic Specialists Conf.*, Kissimmee, FL, Vol. I, May, (1990), pp. 420-423.
46. R. Hartmann, K. -H. Stephan, L. Struder, "The quantum efficiency of pn-detectors from the near infrared to the soft X-ray region", Nuclear Instruments and Methods in Physics Research A, Vol. 439, (2000), pp. 216-220.

Table 1. Level densities N_n, reduced population densities $\frac{N_n}{g_n}$ [a], and overpopulation ratios $\frac{N_n}{N_2}\frac{g_2}{g_n}$, $\frac{N_n}{N_3}\frac{g_3}{g_n}$, and $\frac{N_n}{N_4}\frac{g_4}{g_n}$ for excited states $n=1$ to 9 with an $n>2$ pumping mechanism recorded on a water microwave plasma at 90 W input power.

Principal Quantum Number n	$N_n(10^9\ cm^{-3})$	$\frac{N_n}{g_n}(10^8\ cm^{-3})$	$\frac{N_n}{N_2}\frac{g_2}{g_n}$	$\frac{N_n}{N_3}\frac{g_3}{g_n}$	$\frac{N_n}{N_4}\frac{g_4}{g_n}$
1	60,000 [b]	30,000	—	—	—
2	1.39	1.74	—	—	—
3	6.20	3.44	1.98	—	—
4	28.9	9.02	5.18	2.62	—
5	1930	385	221	112	42.7
6	838	116	66.7	33.7	12.9
7	47.4	4.83	2.78	1.40	0.535
8	26.1	2.04	1.17	0.593	0.226
9	15.3	0.955	0.549	0.278	0.106

[a] $g_n = 2n^2$ and n is the principal quantum number

[b] calculated after ref. [21]

Table 2. Potential laser transitions of atomic hydrogen in a microwave water-vapor plasma.

wavelength/Å	spectral region	electronic transition $n_{initial} - n_{final}$
74,578	IR	$6 \rightarrow 5$
40,512	IR	$5 \rightarrow 4$
26,252	IR	$6 \rightarrow 4$
18,751	IR	$4 \rightarrow 3$
12,818	IR	$5 \rightarrow 3$
10,938	IR	$6 \rightarrow 3$
10,049	IR	$7 \rightarrow 3$
6,563	red	$3 \rightarrow 2$
4,861	blue	$4 \rightarrow 2$
4,340	violet	$5 \rightarrow 2$
4,102	violet	$6 \rightarrow 2$
3,970	violet	$7 \rightarrow 2$
3,889	violet	$8 \rightarrow 2$

Table 3. Observed reduced overpopulation densities recorded on a water microwave plasma at 90 W input power, threshold overpopulation densities for lasing with a 100 cm length cavity, and the minimum laser cavity length to achieve lasing for the observed reduced overpopulation densities for the transitions, 5-2, 5-3, and 6-2.

Laser Transition	ΔE (eV)	Wavelength (Å)	A_{ki} [a] $10^8\ s^{-1}$	Reduced Overpopulation Density $(10^{10}\ cm^{-3})$	Threshold Reduced Overpopulation Density [b] $(10^7\ cm^{-3})$	Minimum Length (cm)
5 - 2	2.86	4340.5	0.0943	3.83	4.61	0.212
5 - 3	0.966	12,818.1	0.0339	3.82	0.494	0.013
6 - 2	3.02	4101.7	0.0515	1.15	6.92	0.605

[a] Einstein A coefficient for the transition from level k to level i

[b] for a laser cavity length of 100 cm and R=0.99

Table 4. Model calculated level densities N_n for excited states $n=1$ to 9 with an $n=3$ to 8 pumping mechanisms.

Principal Quantum Number n	$N_n(10^9\ cm^{-3})$
1[a]	60,000
2	24.4
3	11.7
4	78.4
5[a]	1930
6[a]	838
7	2.3
8	2.5
9	2.6

[a] held fixed at the measured values

Table 5. The pumping rate and pumping power calculated from the collisional-radiative model for laser traditions 5-2, 5-3, and 6-2.

Laser Transition	Calculated Pumping Rate of Upper Level $\left(10^{19}\ cm^{-3}s^{-1}\right)$	Calculated Pumping Power $\left(W \cdot cm^{-3}\right)$
5 - 2	8.4[b]	175.3[a]
5 - 3		
6 - 2	2.12	44.8

[a] for 5-2 and 5-3 transitions

Figure Captions

Figure 1. The experimental set comprising a quartz tube cell, a source of water vapor, a flow system, and a visible spectrometer.

Figure 2. The visible spectrum (4000-6700 Å) of the cell emission from a hydrogen microwave plasma at 90 W input power. No inversion was observed.

Figure 3. The visible spectrum (4000-6700 Å) of the cell emission from a water microwave plasma with 50 W input power. A stationary inverted H Balmer population was observed. The population of the levels $n = 4,5$, and 6 of hydrogen were continuously inverted with respect to $n = 3$.

Figure 4. The visible spectrum (2750-7200 Å) of the cell emission from a water microwave plasma with 90 W input power. A stationary inverted H Balmer population was observed. In addition to the continuous population inversion of the H levels $n = 4,5$, and 6 with respect to $n = 3$ observed at 50 W, the $n = 5$ and 6 levels were further continuously inverted with respect to $n = 4$ when the input power was increased to 90 W. The levels $n = 7,8$, and 9 of hydrogen were also continuously inverted with respect to $n = 3$.

Figure 5. The VUV spectra (900-1300 Å) of the cell emission from hydrogen microwave and water microwave plasmas with 90 W input power. An inverted Lyman population was observed from the water plasma emission with the inversion observed in the visible as shown in Figures 3 and 4 extending to the $n = 2$ level.

Figure 6. The visible spectrum (3000-7200 Å) of the cell emission from an inductively coupled water RF plasma with 90 W input power. No inversion was observed.

Figure 7. The visible spectrum (3000-7200 Å) of the cell emission from a capacitively coupled water RF plasma with 90 W input power. No inversion was observed.

Figure 8. The visible spectrum (2750-7200 Å) of the cell emission from a water high voltage glow discharge plasma with 90 W input power. Strong $OH(A-X)$ emission, but no inversion was observed.

Figure 9. The $OH(A-X)$ microwave water plasma emission spectrum in the region of 2750-3300 Å with 90 W input power.

Figure 10. The $OH(A-X)$ (1-0) R-branch and the (1-0) Q-branch were observed in the 2800-2950 Å region of the microwave water plasma emission spectrum shown in Figure 9.

Figure 11. The $OH(A-X)$ (0-0) R-branch and the (0-0), (1-1), and (2-2) Q-branches were observed in the 3000-3300 Å region of the microwave water plasma emission spectrum shown in Figure 9.

Figure 12. The 6562.8 Å Balmer α line width recorded with a high resolution (±0.06 Å) visible spectrometer on a hydrogen microwave discharge plasma. The statistical curve fit of the Balmer α line width profile matched a Gaussian profile having the $X^2 = \sum \frac{(\text{Calculated} - \text{Measured})^2}{\text{Calculated}}$ and R^2 (correlation coefficient squared) values of 4.86 and 0.99, respectively. No line excessive broadening was observed corresponding to an average hydrogen atom temperature of 1 eV.

Figure 13. The 6562.8 Å Balmer α line width recorded with a high resolution (±0.06 Å) visible spectrometer on a water vapor microwave discharge plasma. The statistical curve fit of the Balmer α line width profile matched a Gaussian profile having the X^2 and R^2 values of 7.48 and 0.996, respectively. Significant broadening was observed corresponding to an average hydrogen atom temperature of 55 eV.

Figure 14. The visible spectrum (3700-3960 Å) of the cell emission from a water microwave plasma with 90 W input power. The catalysis mechanism was supported by the observation of O^{2+} at 3715.0 Å, 3754.8 Å, and 3791.28 Å. O^{+} was observed at 3727.2 Å, 3749.4 Å, 3771 , 3872 Å, and 3946.3 Å. The hydrogen Balmer lines corresponding to the transitions 10-2, 9-2, and 8-2 were also observed.

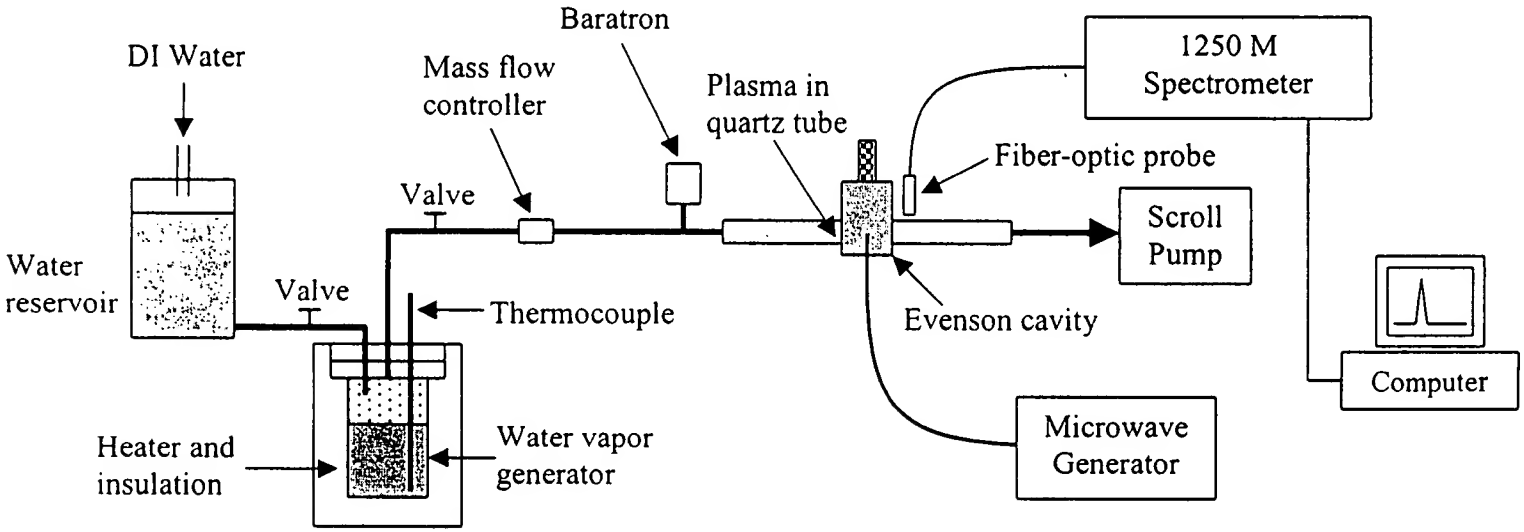
DI Water
Mass flow controller
Baratron
Plasma in quartz tube
1250 M Spectrometer
Fiber-optic probe
Valve
Scroll Pump
Water reservoir
Valve
Thermocouple
Evenson cavity
Computer
Heater and insulation
Water vapor generator
Microwave Generator

Fig. 1

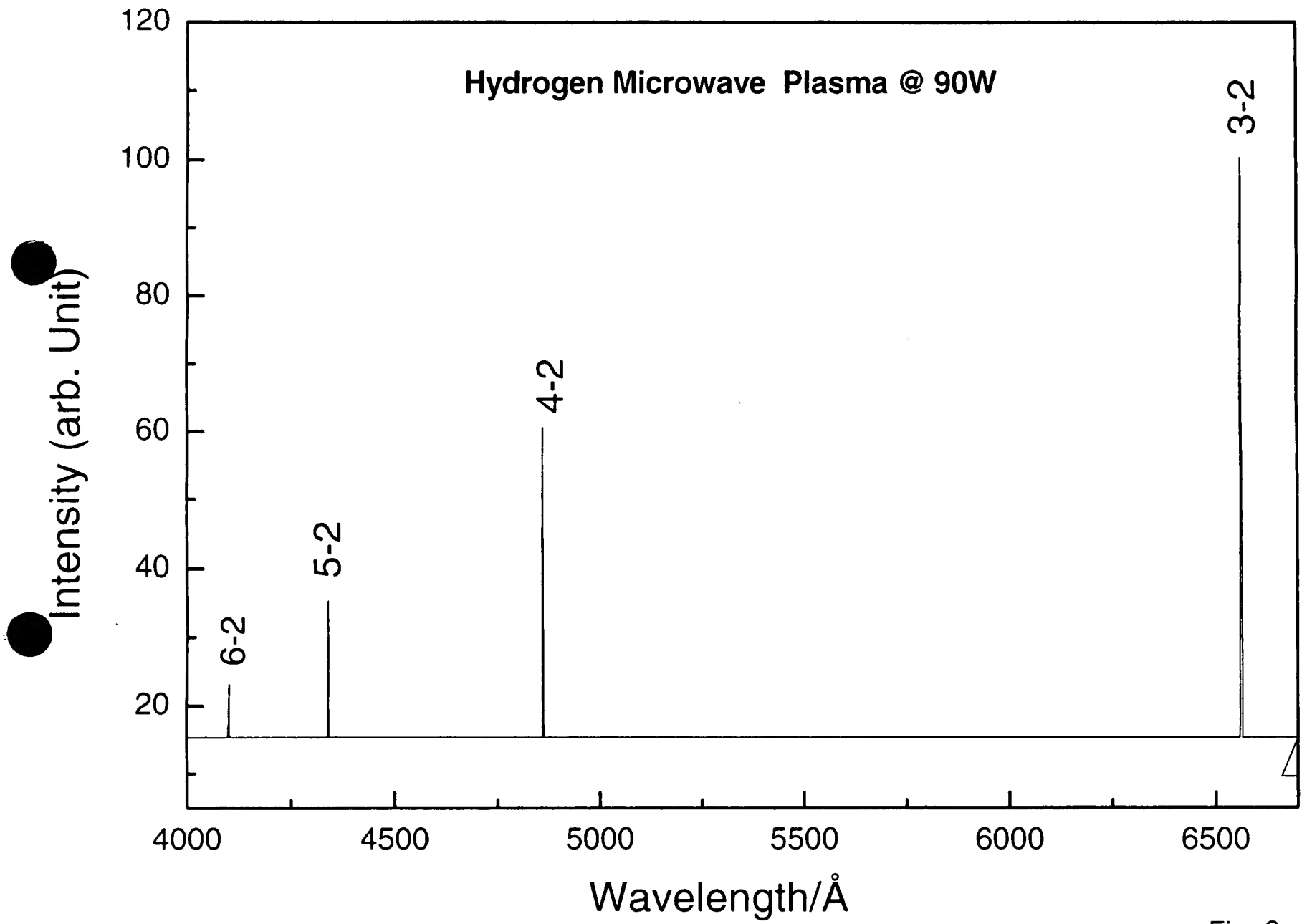
Hydrogen Microwave Plasma @ 90W
Intensity (arb. Unit)
120
100
80
60
40
20
6-2
5-2
4-2
3-2
4000
4500
5000
5500
6000
6500
Wavelength/Å

Fig. 2

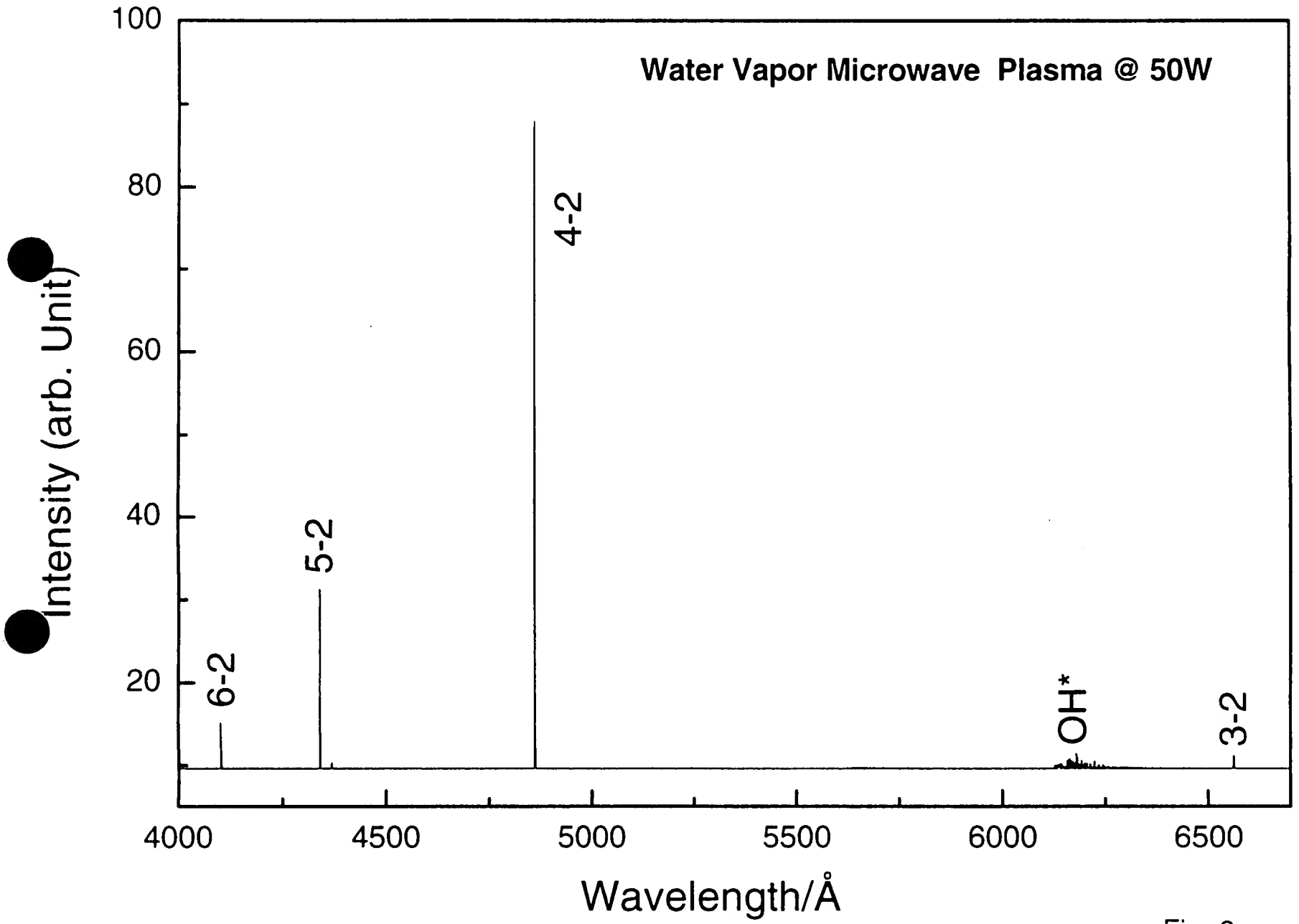
Water Vapor Microwave Plasma @ 50W
Intensity (arb. Unit)
100
80
60
40
20
6-2
5-2
4-2
OH*
3-2
4000
4500
5000
5500
6000
6500
Wavelength/Å

Fig. 3

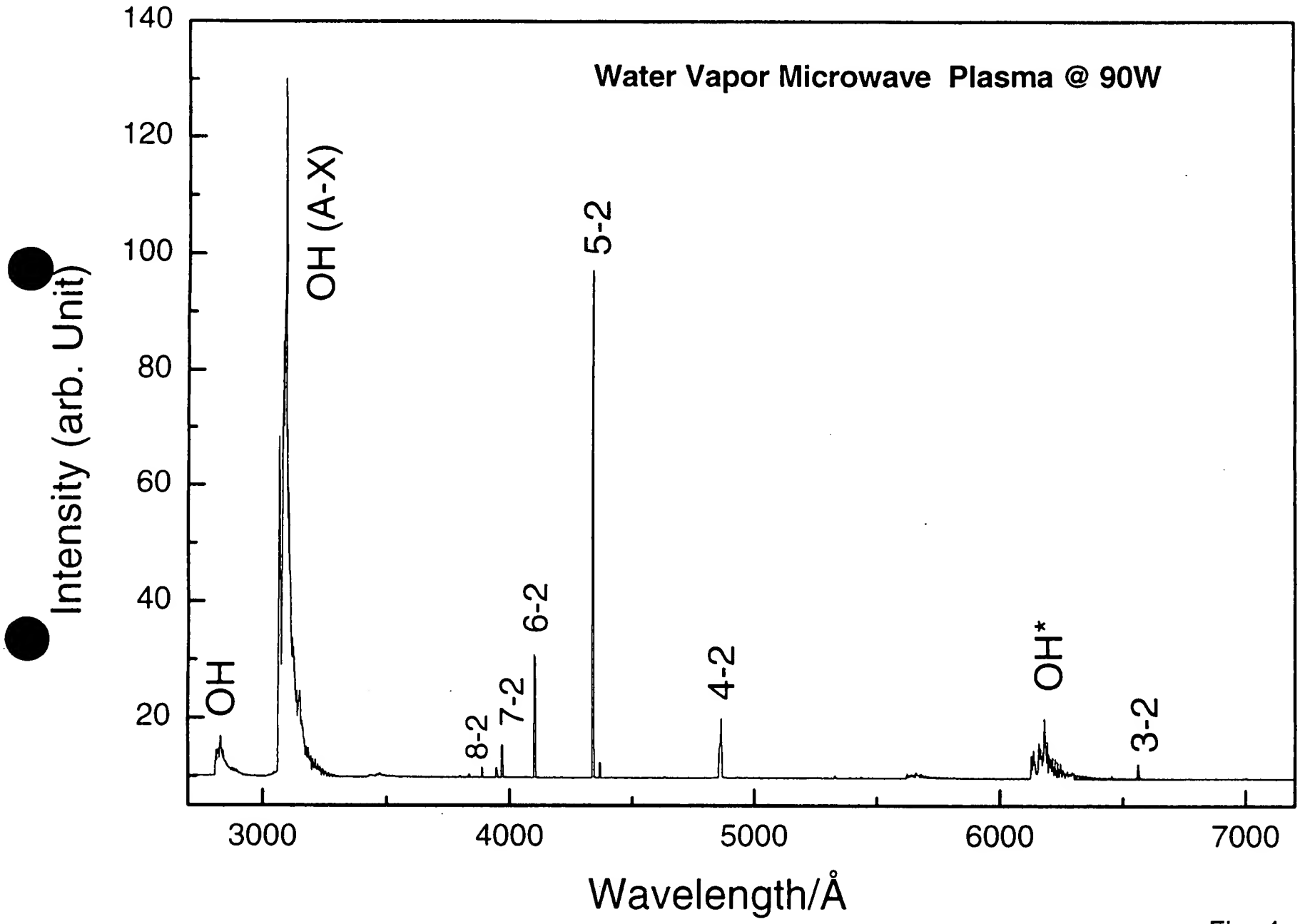
Water Vapor Microwave Plasma @ 90W
Intensity (arb. Unit)
Wavelength/Å
140
120
100
80
60
40
20
3000
4000
5000
6000
7000
OH
OH (A-X)
8-2
7-2
6-2
5-2
4-2
OH*
3-2

Fig. 4

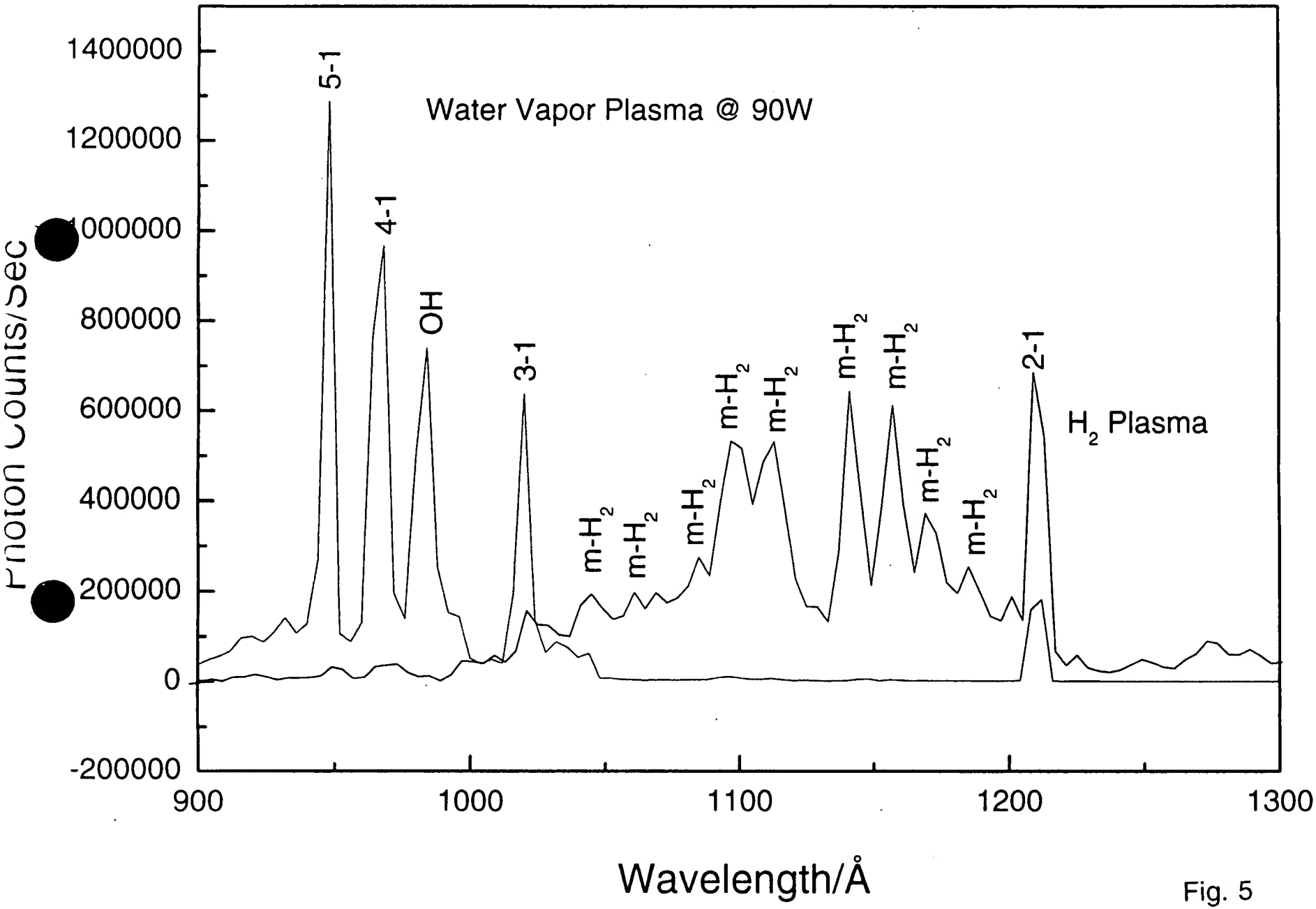
Water Vapor Plasma @ 90W
5-1
4-1
OH
3-1
m-H2
m-H2
m-H2
m-H2
m-H2
m-H2
m-H2
m-H2
2-1
H2 Plasma
Photon Counts/Sec
1400000
1200000
1000000
800000
600000
400000
200000
0
-200000
900
1000
1100
1200
1300
Wavelength/Å

Fig. 5

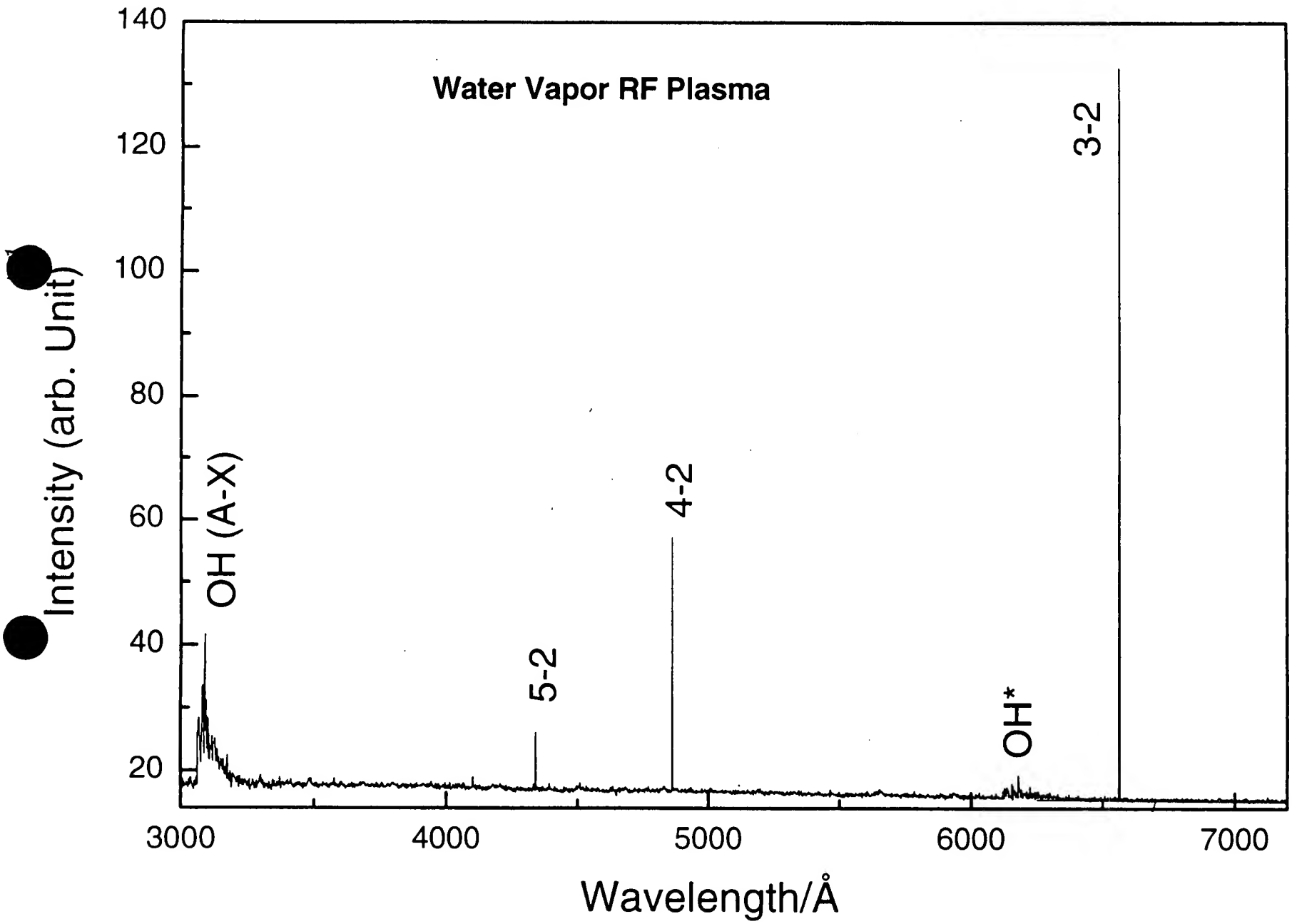
Water Vapor RF Plasma
Intensity (arb. Unit)
Wavelength/Å
140
120
100
80
60
40
20
3000
4000
5000
6000
7000
OH (A-X)
5-2
4-2
OH*
3-2

Fig. 6

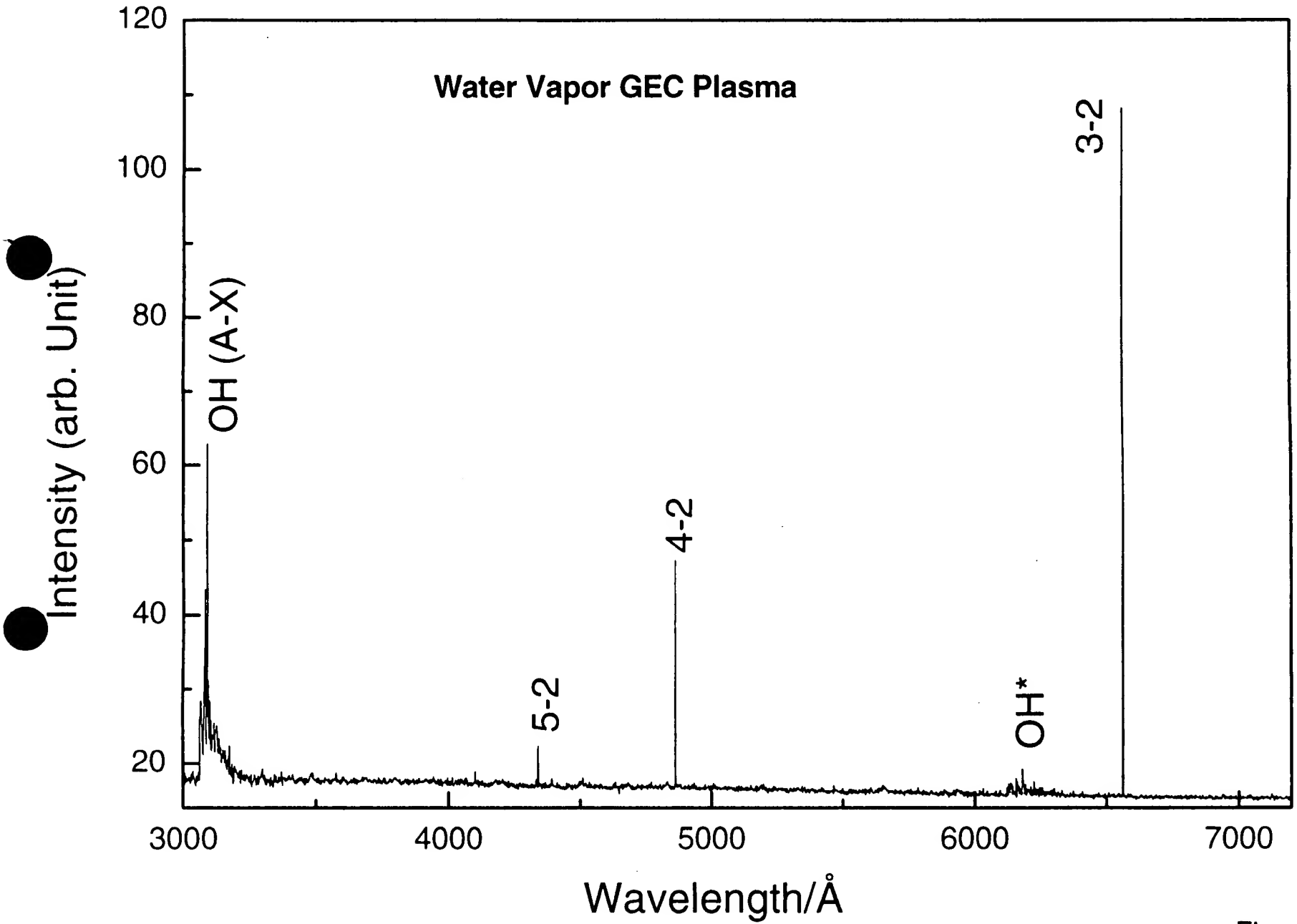
Water Vapor GEC Plasma
Intensity (arb. Unit)
Wavelength/Å
120
100
80
60
40
20
3000
4000
5000
6000
7000
OH (A-X)
5-2
4-2
OH*
3-2

Fig. 7

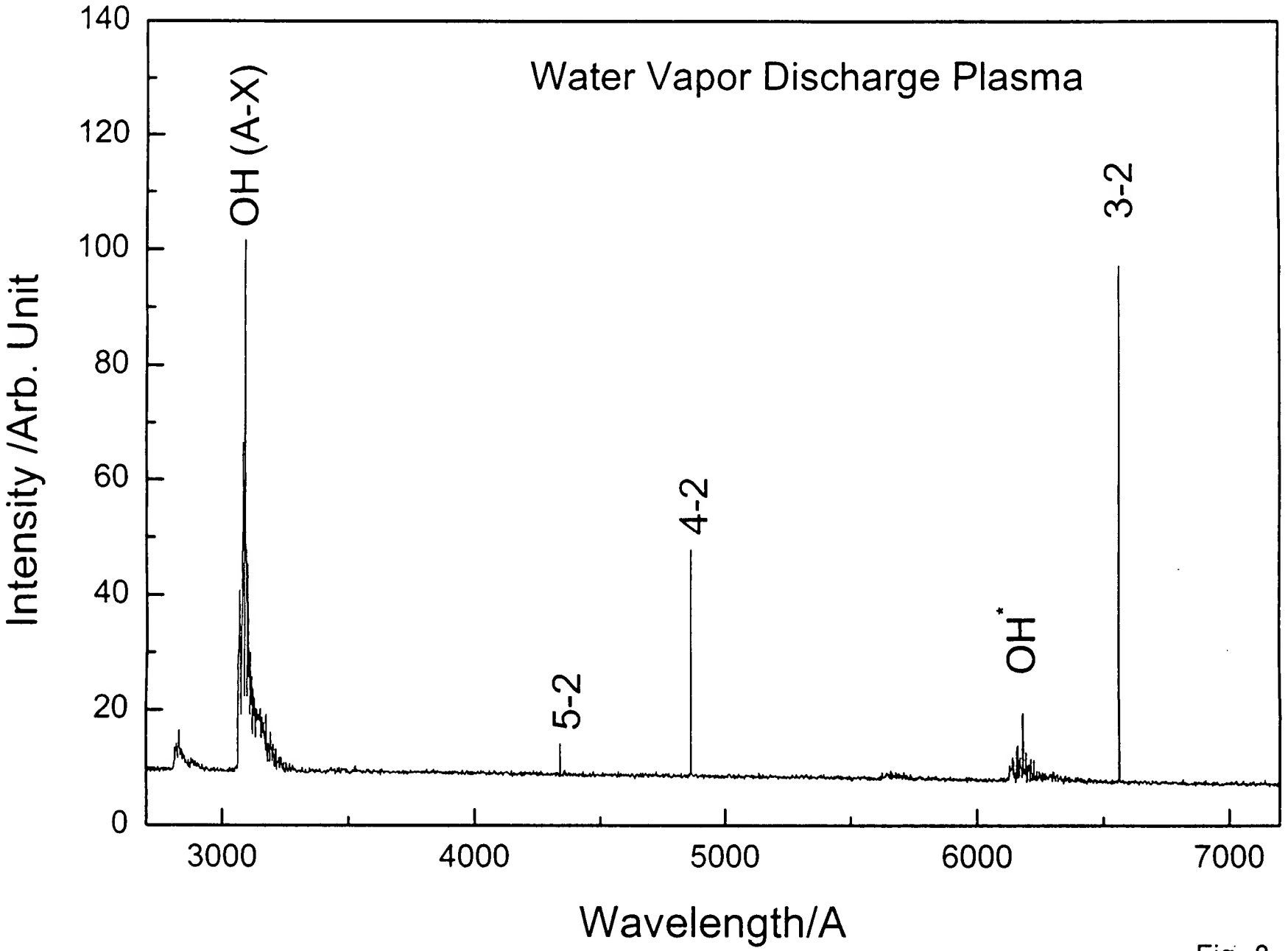
Water Vapor Discharge Plasma
OH (A-X)
5-2
4-2
OH*
3-2
Intensity /Arb. Unit
Wavelength/A
0
20
40
60
80
100
120
140
3000
4000
5000
6000
7000

Fig. 8

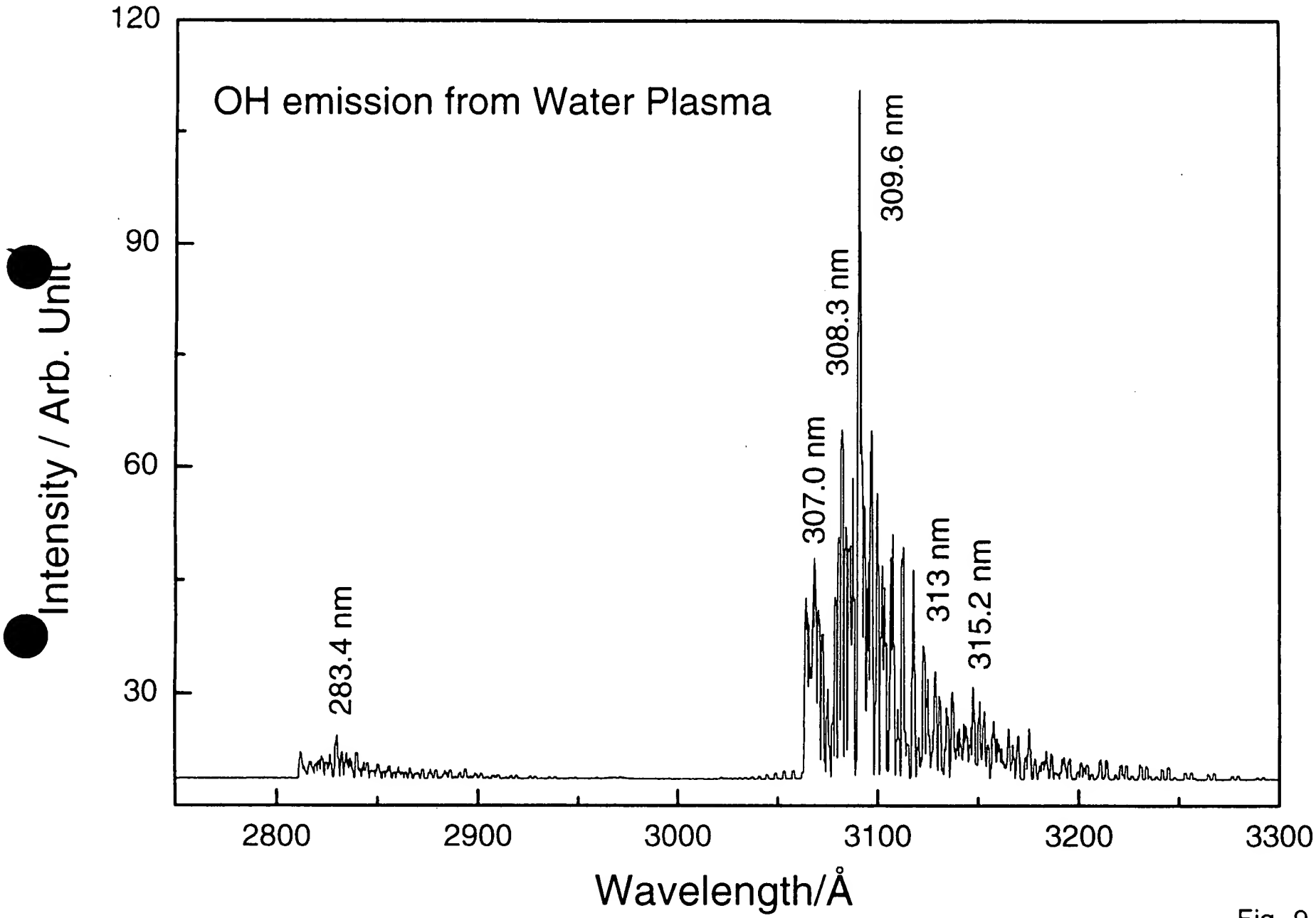
OH emission from Water Plasma
Intensity / Arb. Unit
120
90
60
30
283.4 nm
307.0 nm
308.3 nm
309.6 nm
313 nm
315.2 nm
2800
2900
3000
3100
3200
3300
Wavelength/Å

Fig. 9

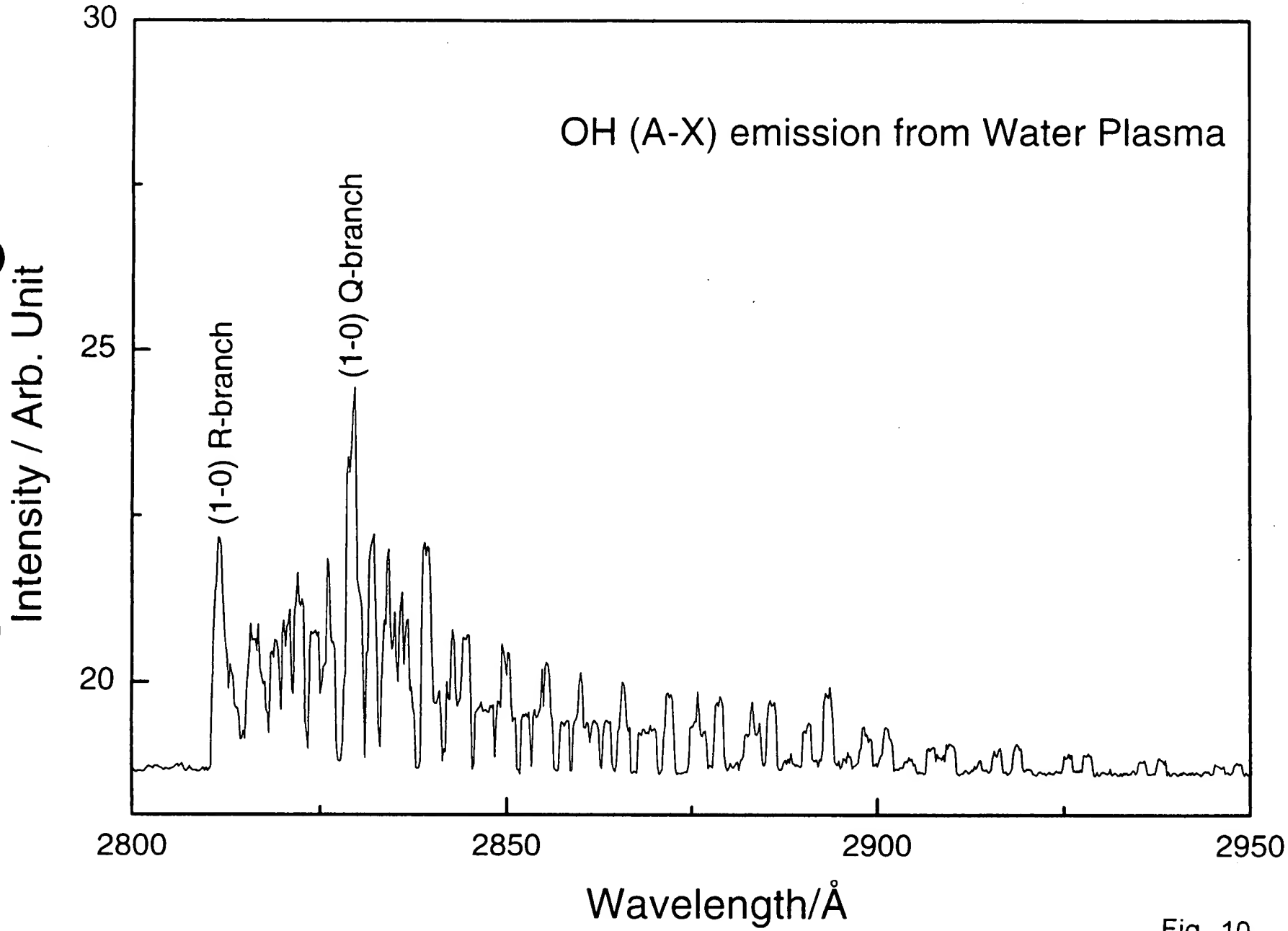
OH (A-X) emission from Water Plasma
(1-0) R-branch
(1-0) Q-branch
Intensity / Arb. Unit
30
25
20
2800
2850
2900
2950
Wavelength/Å

Fig. 10

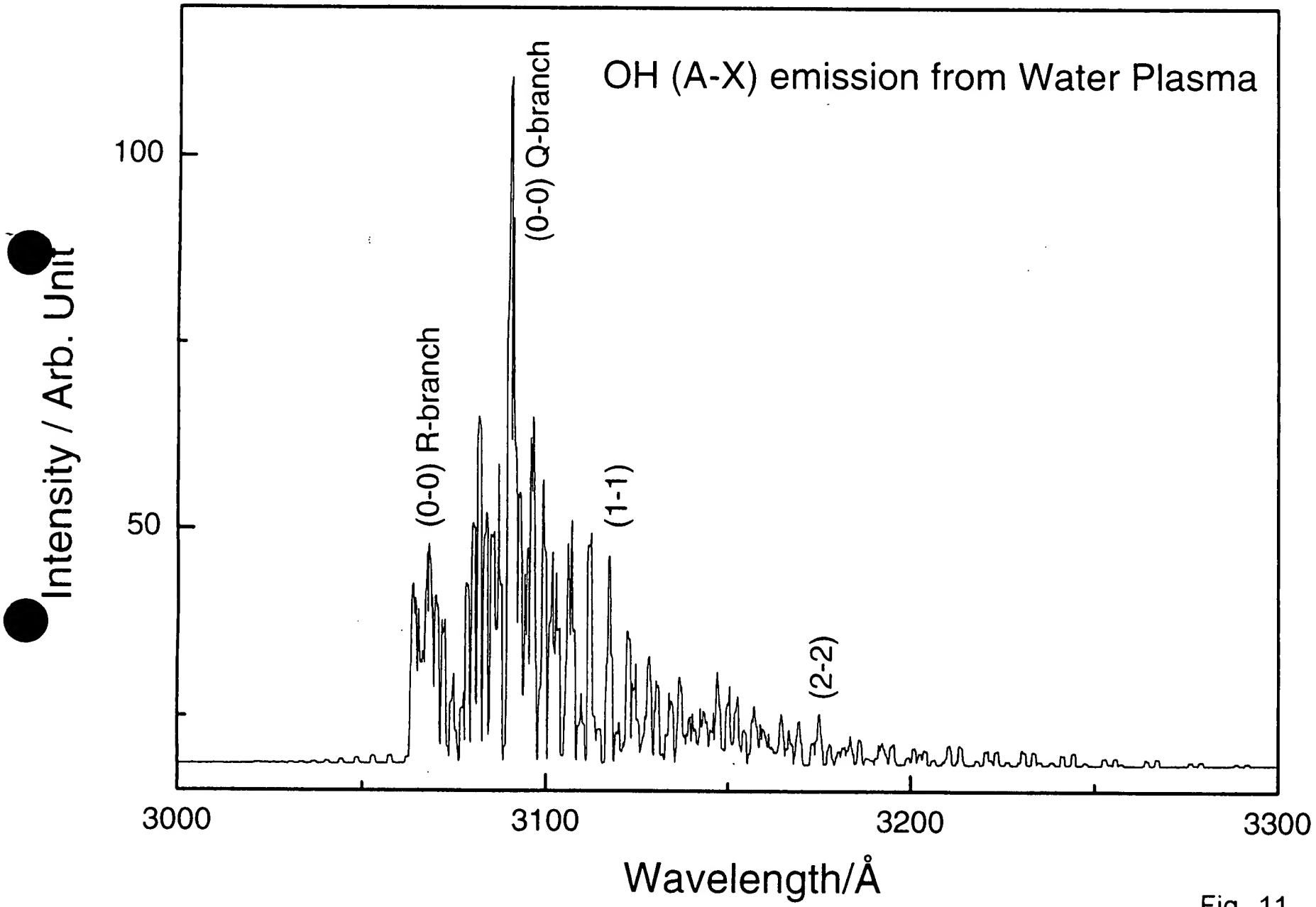
OH (A-X) emission from Water Plasma
(0-0) Q-branch
(0-0) R-branch
(1-1)
(2-2)
100
50
Intensity / Arb. Unit
3000
3100
3200
3300
Wavelength/Å

Fig. 11

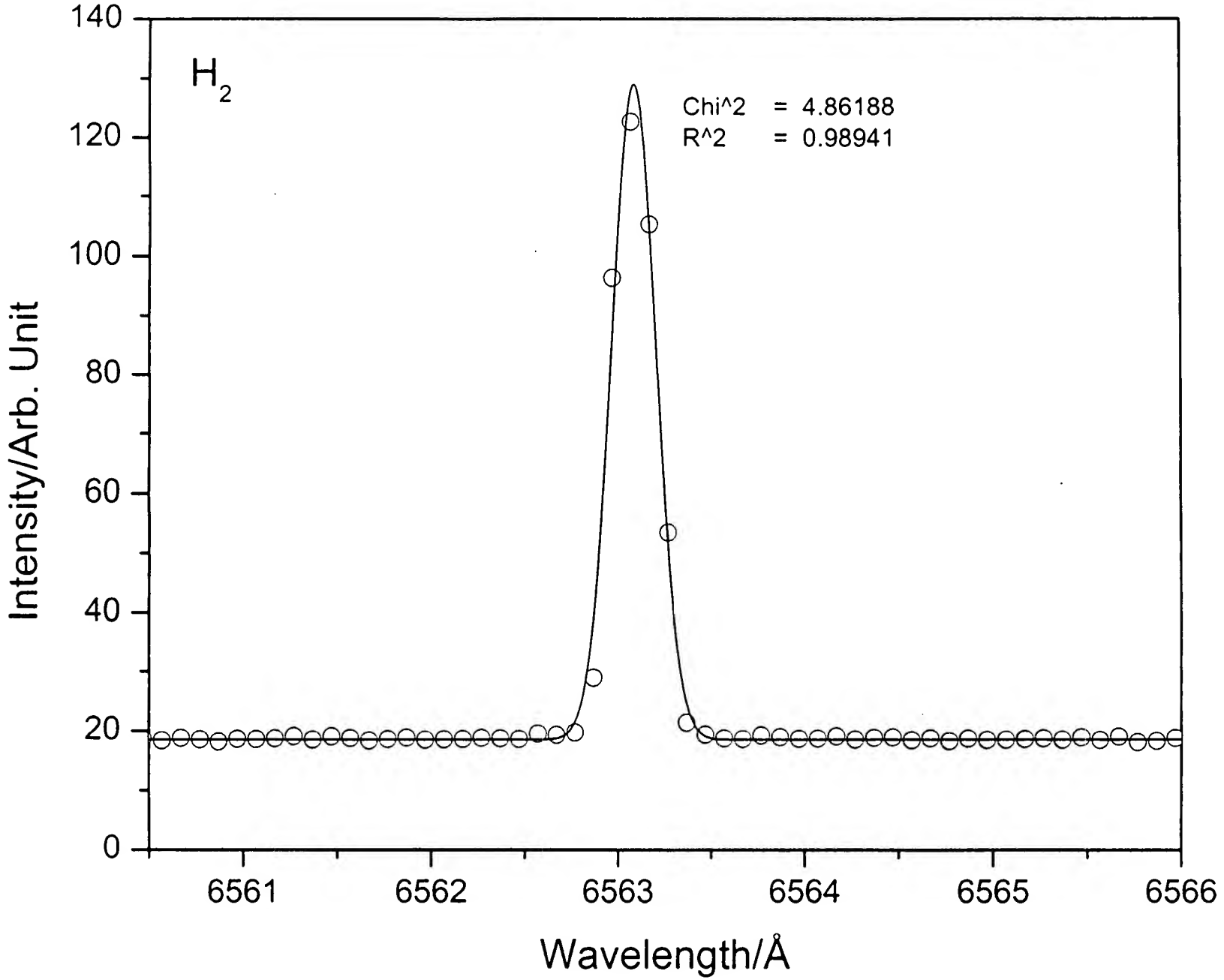
H2
Chi^2 = 4.86188
R^2 = 0.98941
Intensity/Arb. Unit
Wavelength/Å
0
20
40
60
80
100
120
140
6561
6562
6563
6564
6565
6566

Fig. 12

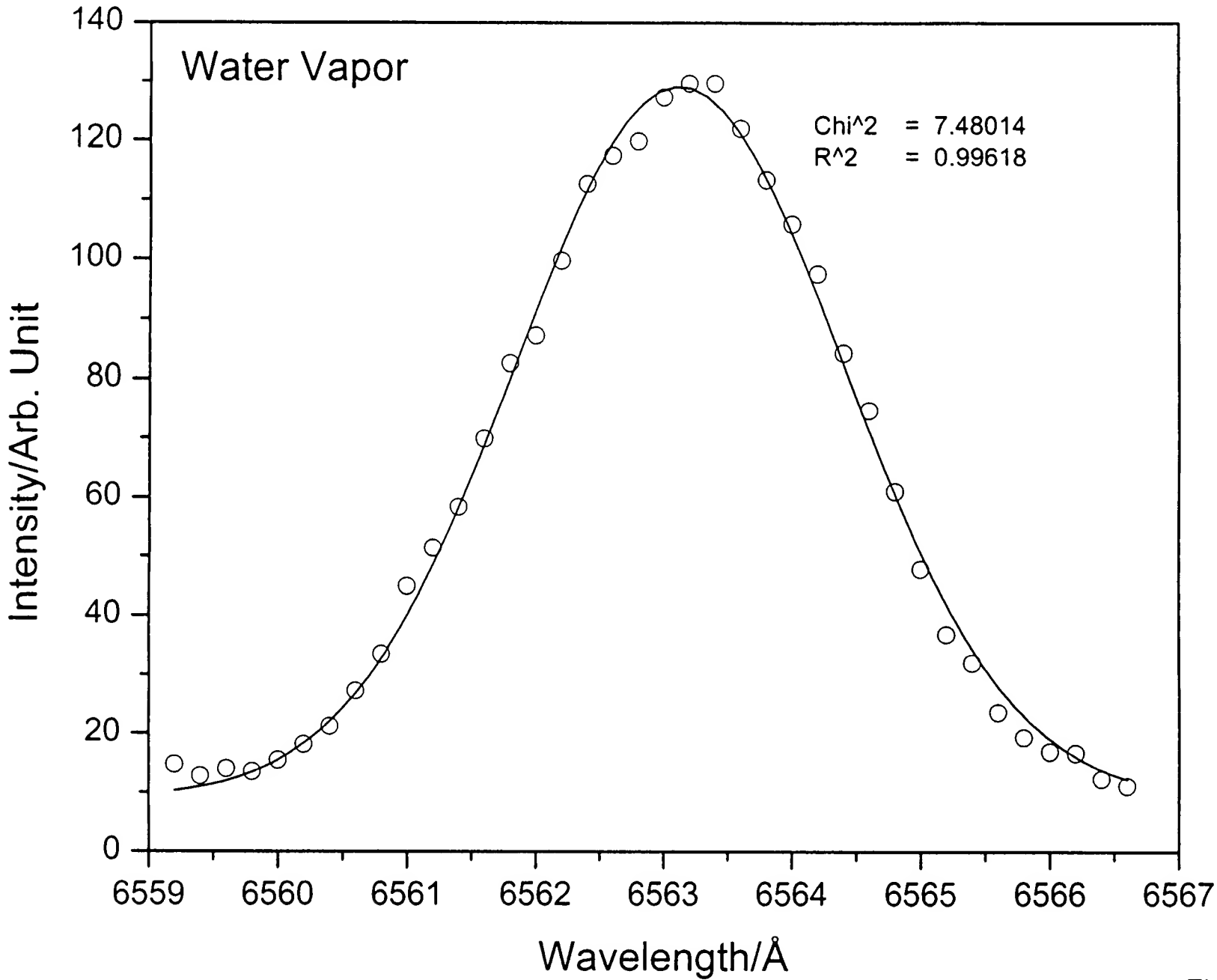
Water Vapor
Chi^2 = 7.48014
R^2 = 0.99618
Intensity/Arb. Unit
Wavelength/Å
0
20
40
60
80
100
120
140
6559
6560
6561
6562
6563
6564
6565
6566
6567

Fig. 13

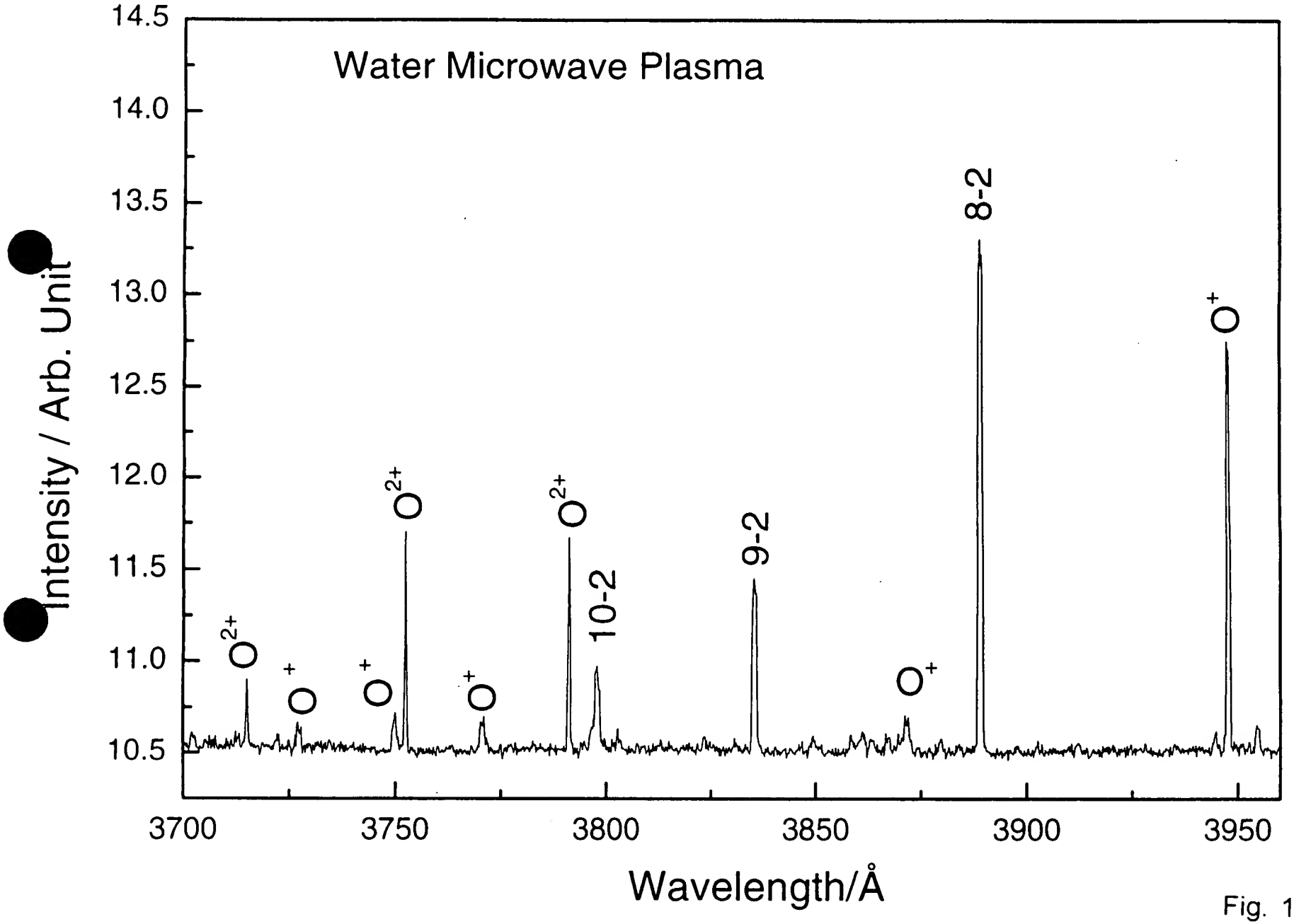
Water Microwave Plasma
Intensity / Arb. Unit
Wavelength/Å
14.5
14.0
13.5
13.0
12.5
12.0
11.5
11.0
10.5
3700
3750
3800
3850
3900
3950
O2+
O+
O+
O2+
O+
O2+
10-2
9-2
O+
8-2
O+

Fig. 14